Composition-Dependent Struggle Between Iodine and Tin Chemistry at the Surface of Mixed Tin/Lead Perovskites

Francesco Ambrosio,[a,b,]* Daniele Meggiolaro,[b] Tahani M. Almutairi,[d] Filippo De Angelis [a,b,c]*

[a]*CompuNet, Istituto Italiano di Tecnologia, Via Morego 30, 16163 Genova, Italy.*

[b]*Computational Laboratory for Hybrid/Organic Photovoltaics (CLHYO), Istituto CNR di Scienze e Tecnologie Chimiche "Giulio Natta" (CNR-SCITEC), Via Elce di Sotto 8, 06123 Perugia, Italy.*

[c]*Department of Chemistry, Biology and Biotechnology, University of Perugia, Via Elce di Sotto 8, 06123 Perugia, Italy.*

[d] *Chemistry Department, College of Science, King Saud University, Riyadh 11451, Saudi Arabia.*

*E-mail: Francesco.Ambrosio@iit.it, filippo@thch.unipg.it

Abstract

Tin alloying is one of the most promising strategies to reduce lead content in metal halide perovskites solar cells. In fact, mixed tin-lead perovskites have shown photoconversion efficiencies comparable to those of full lead-based perovskites and improved long-term stability with respect to tin perovskites. We here demonstrate, through advanced *ab initio* calculations, that the recent success of mixed perovskites lies in a composition-dependent struggle between tin and iodine chemistry at the surface of the material. In particular, we prove that the oxidation of surface Sn(II) to Sn(IV), which condemns tin halide perovskites with low photo-conversion efficiency and thermodynamic instability, is hindered at the surface of mixed $MAPb_{0.5}Sn_{0.5}I_3$ by the competition with iodine-related defects in both pristine and defective models. In particular, iodine-related defects are found to be generally favoured by both thermodynamics and kinetics while surface Sn(IV) can be promoted only under Sn poor conditions. However, when Sn is alloyed in low concentration, it act as a dopant in the lead perovskite and Sn(IV) is promptly formed on the surface of the perovskite. By explaining the effect of tin/lead alloying on both stability and opto-electronic properties of the material, we provide a rationale beyond the experimental strategies currently employed to synthetize mixed tin/lead perovskites.

TOC Figure

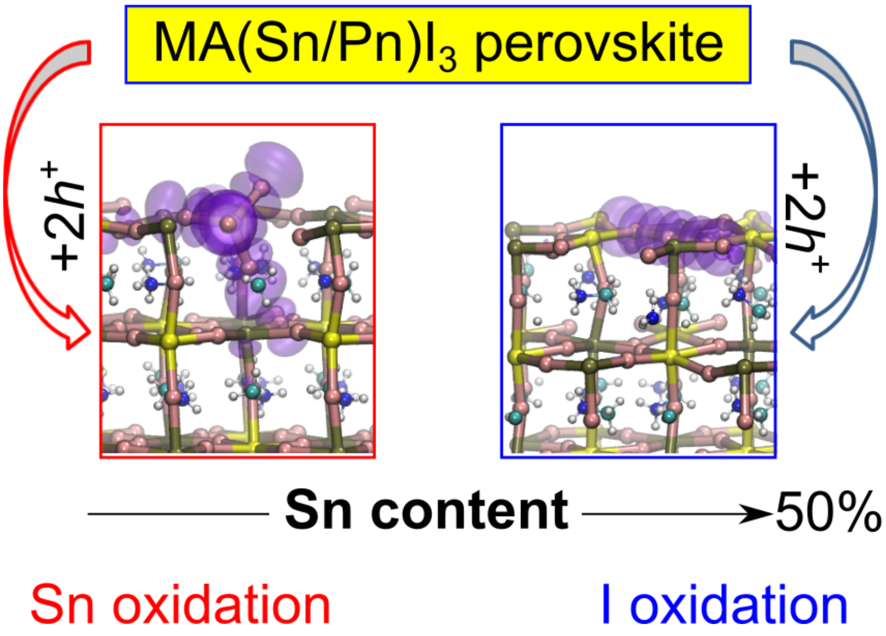
MA(Sn/Pn)I$_3$ perovskite
+2h^+
+2h^+
Sn content
50%
Sn oxidation
I oxidation

Metal halide perovskites are the most promising candidates for future photovoltaics industry by virtue of their outstanding optoelectronic properties.[1-7] The most performing devices, with photo-conversion efficiencies above 25%, are based on lead halide perovskites (LHPs)[8] which have indeed received most of the attention by the scientific community in the last ten years. The characterization of the remarkable properties of LHPs, such as the slow bimolecular recombination coefficients[9-15]and defect tolerance, [16-23] has provided valuable advancements from a basic science perspective. However, being lead a toxic element,[24, 25] the introduction in the mass-market of devices containing this element in sizable concentrations poses serious problems, also in view of the ongoing efforts to reduce the impact of anthropization. For this reason, while strategies to recycle lead in non-aqueous environment have been recently explored[26] and strategies to reduce the dimensionality and the depth of the perovskite thin films have been deployed,[27, 28] replacement or reduction of lead content in the perovskite by substitution with less toxic elements *while* retaining the optoelectronic properties observed for LHPs represents a compelling challenge in this research field.[29]

Currently tin is the only viable alternative to lead with significant efficiency[30, 31] among those investigated: e.g. germanium[32], combinations of I/III metals such as Bi and Ag.[33-35] While tin halide perovskites (THPs) possess interesting optoelectronic properties, such as low exciton binding energies and lower band gaps compared to LHPs,[36-38] photoconversion efficiencies only up to ~13% have been recorded.[39-41] Such performance gap with LHPs originates from the self-p-doping characteristics of THPs, which, coupled to the facile oxidation of Sn(II) to Sn(IV), ultimately leads to enhanced non-radiative recombination and thermodynamic instability of the material.[31, 42-46] As recently reported, the heavy THPs p-doping favours the nucleation of surface Sn(IV) centers which, in turn, act as electron traps that promote recombination and lattice degradation towards secondary phases, *e.g.* MA_2SnI_6 and SnI_4 for $MASnI_3$ (MA=methylammonium).[46]

Recently, promising results have been obtained for mixed tin/lead perovskites which have shown solar to electrical power conversion efficiencies up to 20%.[47-49] These encouraging developments indicate that such systems could become competitive with LHPs. The key factors favouring the use of mixed perovskites are their tunable band gap [44, 50] and their peculiar defect chemistry.[45] In fact, density functional theory (DFT) calculations demonstrated that the defect activity in lead (tin) iodide perovskites is dominated by iodine (tin) chemistry, which is responsible of the formation of deep hole (electron) traps.[45] In contrast, 50:50 tin/lead perovskites show an intermediate behaviour which could possibly makes them potentially free of deep traps.[45] Furthermore, the more intrinsic nature of $MAPb_{0.5}Sn_{0.5}I_{3}$,[45] with the Fermi level lying 0.4 eV above the valence band, may partially suppress tin oxidation.[46]

One may actually note that LHPs are already defect-tolerant [16 17-23] . This is indeed true for the bulk material, due to the combined effects of energy barriers associated with hole trapping and the polaronic nature of the charge carriers,[14] which reduces the probability of defect-mediated recombination.[51] However, charge recombination at the surface of LHPs[52, 53,54] can play a major role in undermining the performance of the device and initiating the degradation of the material.[55, 56] It is, therefore, quintessential to appropriately tailor the surface properties of LHPs to curtail these noxious phenomena.[57] In this regard, passivation strategies have been successfully deployed to deactivate surface defect states with a beneficial impact on the photo-conversion efficiency.[58-62] In contrast, the role of defects at the surface of mixed tin/lead perovskites has not received comparable attention. Experiments have shown that low contents of Sn in the perovskite (0.5-20%) translate into poor optoelectronic properties with a dramatic increase in non-radiative recombination.[63] At variance with this, surface treatments, such as vacuum-assisted growth and annealing,[64, 65] addition of passivating layers,[66] and inclusion of excess Sn powder in the precursor solution[48] were found to be beneficial in reducing the concentration of surface traps. A comprehensive understanding on the electronic properties and the defect chemistry of mixed tin/lead perovskites is thus highly desirable to further boost the optoelectronic quality of these lead-alleviated materials.

In this Letter, we unveil a composition-dependent competition between tin and iodine defect activity at the surface of mixed tin/lead perovskites. By means of advanced *ab initio* calculations we show that formation of surface Sn(IV), at the root of the poor efficiency and of the instability of tin halide perovskites, is hindered in $MAPb_{0.5}Sn_{0.5}I_3$ by the struggle between tin and iodine chemistry, with beneficial effects on the material's optoelectronic properties and, in turn, on the long-term stability. In stark contrast, alloys with low tin content are dramatically affected by tin oxidation, thus explaining the observed opto-electronic properties measured in recent experiments.

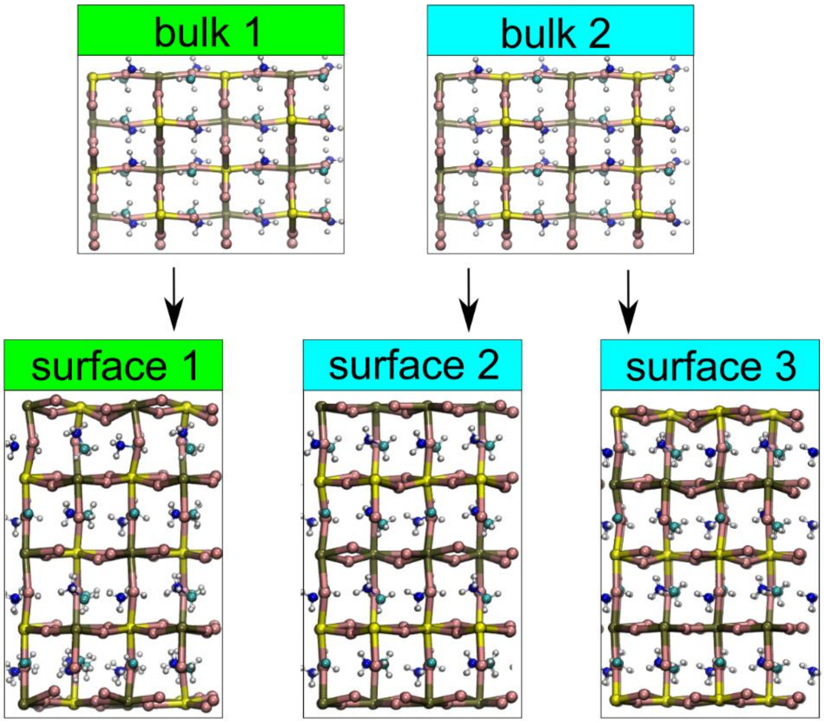

Figure 1. Schematic representation of the bulk models of $MAPb_{0.5}Sn_{0.5}I_3$ and the related (001) surfaces. Pb atoms are given in brown, Sn in yellow, I in pink, C in cyan, N in blue, and H in white.

The tetragonal axis lies horizontally for bulk models while a view with the *z* axis lying vertically is represented for the slabs.

We perform hybrid-DFT calculations (cf. Supplementary Information) on MI_2–terminated (M=Sn/Pb) (001) surfaces of $MAPb_{0.5}Sn_{0.5}I_3$ as such unpassivated systems serve as extreme examples of surface chemistry in mixed tin/lead compounds. We do not include MAI covered surfaces as they have shown low reactivity and bulk-like electronic properties in both LHPs and THPs.[46, 55] We first consider two bulk models: (i) one in which $Pb_{0.5}Sn_{0.5}I_2$ planes occur along the *c* direction and (ii) one in which layers of PbI_2 and SnI_2 are alternated along the *c* direction (bulk 1 and bulk 2 respectively from Fig. 1, cf Supplementary Information for details). Bulk 2 is calculated to be 0.08 eV more stable than bulk 1 in line with previous estimates.[67] From bulk 1, we construct a stoichiometric apolar (001)-$Pb_{0.5}Sn_{0.5}I_2$ terminated slab (surface 1). From bulk 2, we construct symmetric SnI_2-terminated (surface 2) and PbI_2-terminated slabs (surface 3), which represent two limit conditions of full Pb and Sn coverage, respectively (cf. Fig. 1). These models are apolar but their Pb:Sn ratio is either 0.6:0.4

or 0.4:0.6. Therefore, we here focus on the stoichiometric surface 1 while surface 2 and 3 are discussed in the Supplementary Information.

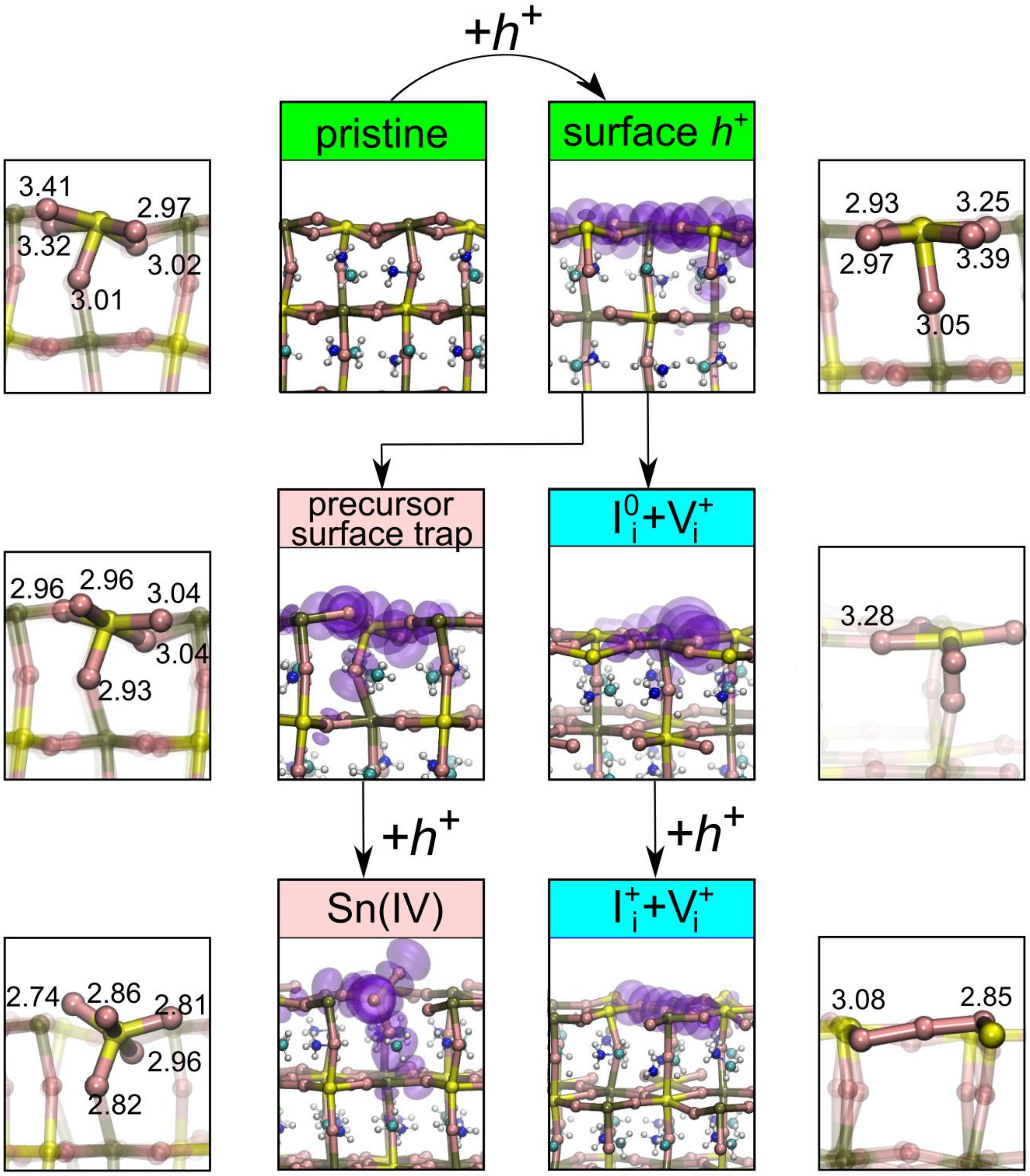

Figure 2. Schematic representation of hole-trapping species on the pristine (001) surface 1 model of $MAPb_{0.5}Sn_{0.5}I_3$. Pb atoms are given in brown, Sn in yellow, I in pink, C in cyan, N in blue, and H in white, isodensity representation of the hole in purple. The z axis lies vertically. For the precursor surface trap and Sn(IV), we provide the Sn-I bond lengths of the involved Sn atom the to be compared

to those calculated for a surface Sn on the neutral and positively charged pristine slab. For the iodide dimer and trimer, we provide the respective bond lengths. All values are given in Å.

As a first step, we investigate the self-trapping process of holes on the pristine surface. Our calculations show that charge localization can occur in three different ways upon injection of a single hole into the system (cf. Fig. 2):

(i) formation a surface hole polaron with binding energy of 0.19 eV, a value slightly larger than that estimated for the bulk (cf. Supplementary Information) and in line with previous results on the PbI_2-terminated $MAPbI_3$ surface.[55]

(ii) formation of a so-called a V-center,[68] a typical defect occurring in metal halides.[69-71] This is originated by the displacement of a neutralized iodine from its lattice site to form a bridging I_2^- dimer with a bond length of 3.28 Å (*i.e.* a neutral interstitial iodine I_i^0, cf. Fig. 2) and a positively charged iodine vacancy V_I^+:

$$\mathrm{MAPb_{0.5}Sn_{0.5}I_3} + h^+ \rightarrow \mathrm{I}_i^0 + \mathrm{V}_\mathrm{I}^+ \qquad (1)$$

(iii) hole trapping on a distorted surface SnI_5^-, upon contraption of Sn-I bonds by ∼0.1 up to 0.3 Å with respect to the neutral system (cf. Fig. 2). This structure represents a precursor to the formation of surface Sn(IV) previously encountered in tin perovskites.[46]

The surface hole polaron is promptly formed upon structural relaxation of the slab with an extra hole. Furthermore, it is found to be slightly more stable than the V-center (precursor trap state) by 0.19 (0.10) eV. Linear transit calculations (cf. Supplementary Information),[72] indicate that the surface polaron →

V-center (precursor trap state) charge localization process entails an energy barrier of 0.26 (0.24) meV [cf. Fig. 3 (a)].

We then consider the trapping of a second hole. For the system bearing the V-center, we observe the spontaneous formation of an interstitial/vacancy $\mathrm{I}_i^+/\mathrm{V}_\mathrm{I}^+$ iodine Frenkel defect (IFD) [73] (cf. Fig. 2), via the following reaction:

$$\mathrm{I}_i^0 + \mathrm{V}_\mathrm{I}^+ + h^+ \rightarrow \mathrm{V}_\mathrm{I}^+ + \mathrm{I}_i^+, \qquad (2)$$

in which the formation of a positively charged interstitial iodine (I_i^+), formally an I_3^- moiety, is envisaged. Direct IFD formation by capture of two holes from the pristine perovskite via:

$$\mathrm{MAPb_{0.5}Sn_{0.5}I_3} + 2h^+ \rightarrow \mathrm{V}_\mathrm{I}^+ + \mathrm{I}_i^+, \qquad (3)$$

is e energetically favourable by 0.81 eV. However, a substantial energy barrier [0.74 eV, cf Fig 3(b)] is associated with reaction (3). Therefore, the occurrence of the IFD is likely subdued to that of the V-center. Similarly, injection of a second hole onto the precursor trap state leads to Sn(IV) with further contraption of the Sn-I bonds. Direct Sn(IV) formation via:

$$\mathrm{MAPb_{0.5}Sn_{0.5}I_3} + 2h^+ \rightarrow \mathrm{Sn(IV)_{surf}}, \qquad (4)$$

while being exothermic by 0.89 eV, is also hindered by a significant energy barrier [cf. Fig. 3 (b)].

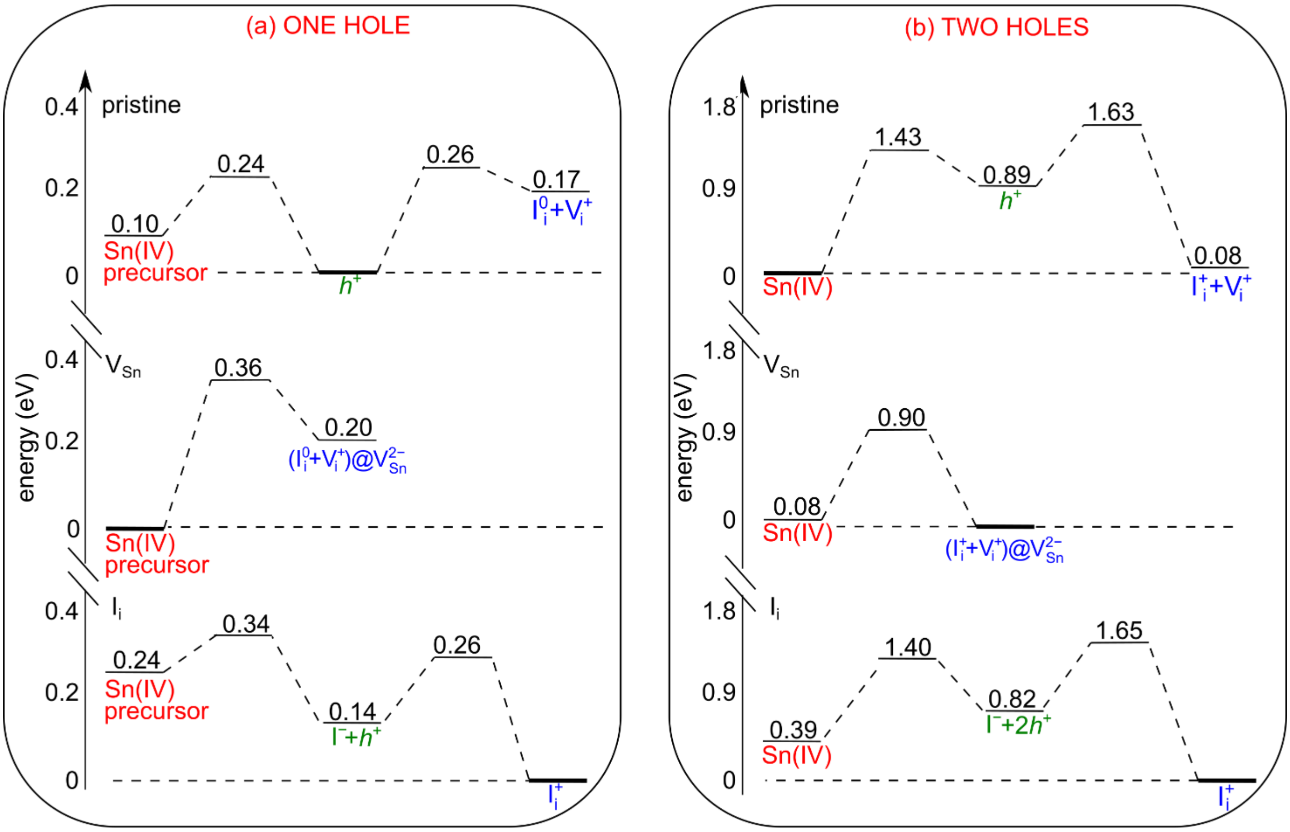

Figure 3. Energy diagrams of species trapping (a) one hole and (b) two holes on the pristine (001) surface 1 model of $\mathrm{MAPb_{0.5}Sn_{0.5}I_3}$ and on the surface bearing a Sn vacancy and an interstitial I. In each diagram, energies are referred to that of the most stable species, which is highlighted with a thicker horizontal line.

So far, our analysis suggests a competition between iodine and tin defects for trapping photo-generated holes, with almost iso-energetic pathways. The precursor step to IFD formation is the capture of a hole on the V-center, which is moderately unfavourable by both kinetics and thermodynamics (cf. Fig. 3). Tin oxidation is also disadvantaged for similar reasons, as the surface trap which is a precursor to Sn(IV) is likewise metastable and its occurrence implies overcoming an energy barrier. Furthermore, the simultaneous trapping of two holes for both IFD and Sn(IV) is strongly hindered by kinetics. These results, combined with the mild p-doped electronic nature of $MAPb_{0.5}Sn_{0.5}I_3$ characterized by a Fermi level predicted at 0.4 eV above the VB,[45] indicate that both IFDs and Sn(IV) are unlikely to be formed even on a highly reactive unpassivated surface. This is at variance with $MASnI_3$, where the heavy p-doping may promote the spontaneous oxidation of tin and the degradation of the material.[45, 46]

The delicate equilibrium between iodine and tin chemistry at the surface of mixed tin/lead perovskites can be perturbed when considering common point defects in the material, such as I interstitials and Sn vacancies. In $MAPbI_3$ both I and Pb defects are notably related to iodine chemistry: in fact, Pb vacancies stabilize the formation of neutral and positively charge interstitial iodine (again, related to formation of I_2^- and I_3^- moieties, respectively) when occurring at the vacancy site. A similar phenomenon is observed upon interaction between lattice iodine and interstitial iodine.[55, 56] However, Sn vacancies at the $MASnI_3$ surface were found to induce the oxidation of unsaturated Sn(II) to Sn(IV).[46] Therefore, both excess iodine and the presence of undercoordinated surface Sn atoms may modify the physical picture observed for the pristine surface.

We first investigate hole trapping mediated by a Sn vacancy (V_{Sn}). For a slab bearing a V_{Sn}^{2-}, we have two distinct possibilities for hole localization (cf. Supplementary Information for detailed structures):

(i) formation of a V-center at the Sn vacancy site.

(ii) hole trapping at a surface Sn(IV) precursor.

Upon injection of a hole on the slab with a V_{Sn}^{2-}, we observe spontaneous localization on the Sn(IV) precursor which is 0.20 eV more stable than the V-center. An energy barrier of 0.36 eV is estimated for the associated Sn(IV) precursor/ V-center charge transfer reaction [cf. Fig. 3(a)]. Again, the formation of an IFD is spontaneously observed upon inclusion of a second hole into the V-center, while the precursor evolves towards surface Sn(IV) (cf. Supplementary Information). The IFD on the vacancy site is found to be 0.08 eV more stable than Sn(IV). As previously noted for $MAPbI_3$,[74] the presence of a metal vacancy facilitates the interaction between neighbouring lattice iodine atoms. However, in the present case, the first injected hole is preferentially trapped on the surface Sn(IV) precursor, thus favouring the reaction pathway leading to tin oxidation. Furthermore, the $\mathrm{Sn(IV)} \rightarrow \mathrm{I_i^+@V_{Sn}^{2-}}$ reaction (*i.e.* reduction of tin and oxidation of iodide) is curbed by a sizable energy barrier [∼1 eV, cf. Fig. 3(b)] due to the large structural differences among the two systems. Overall, these results denote that tin oxidation is reinforced by the Sn vacancy.

We then consider hole-trapping mechanisms assisted by an interstitial iodine defect (cf. Supplementary Information for details of the structural models). Starting from $\mathrm{I_i^-}$, addition of a single hole can lead to:

(i) formation of a surface polaron (*i.e.* no trapping on the defect as in the pristine slab).

(ii) formation of a metal-bridging dimer (the so-called H-center, $\mathrm{I_i^0}$) between a lattice I and and interstitial I upon capture of a single hole by $\mathrm{I_i^-}$.[25]

(iii) hole trapping at a surface Sn(IV) precursor.

Introduction of a single hole on the $\mathrm{I_i^-}$ system results in polaron formation. However, the H-center ($\mathrm{I_i^0}$) is here found to be the most stable moiety, its energy being 0.14 (0.24) eV lower than that of the surface polaron [Sn(IV) precursor)]. Furthermore, the surface polaron → H-center reaction is subject to only a low energy barrier of 0.12 eV [cf. Fig. 3(a)]. In contrast, the Sn(IV) precursor is the least stable of the considered species. Again, I_3^- (corresponding to $\mathrm{I_i^+}$) spontaneously appears when adding a second hole to the H-center while Sn(IV) is achieved from the precursor trap state, the former being 0.39 eV more stable than the latter. These results clearly highlight how interstitial iodine defects dramatically shift the balance towards the prevalence of iodine chemistry.

Overall, the competition between iodine and tin chemistry in determining the electronic properties of the mixed perovskite is modulated by defects. In fact, for the undefective system, a single hole is preferentially localized on the surface as a hole polaron, thus hampering charge-trapping pathways leading either to surface tri-iodide or Sn(IV). This balance can be shifted towards tin and iodide oxidation by V_{Sn} and I_i, respectively. Such results suggest that the opto-electronic properties of the mixed perovskite can be actually tailored by choosing adequate growth conditions.

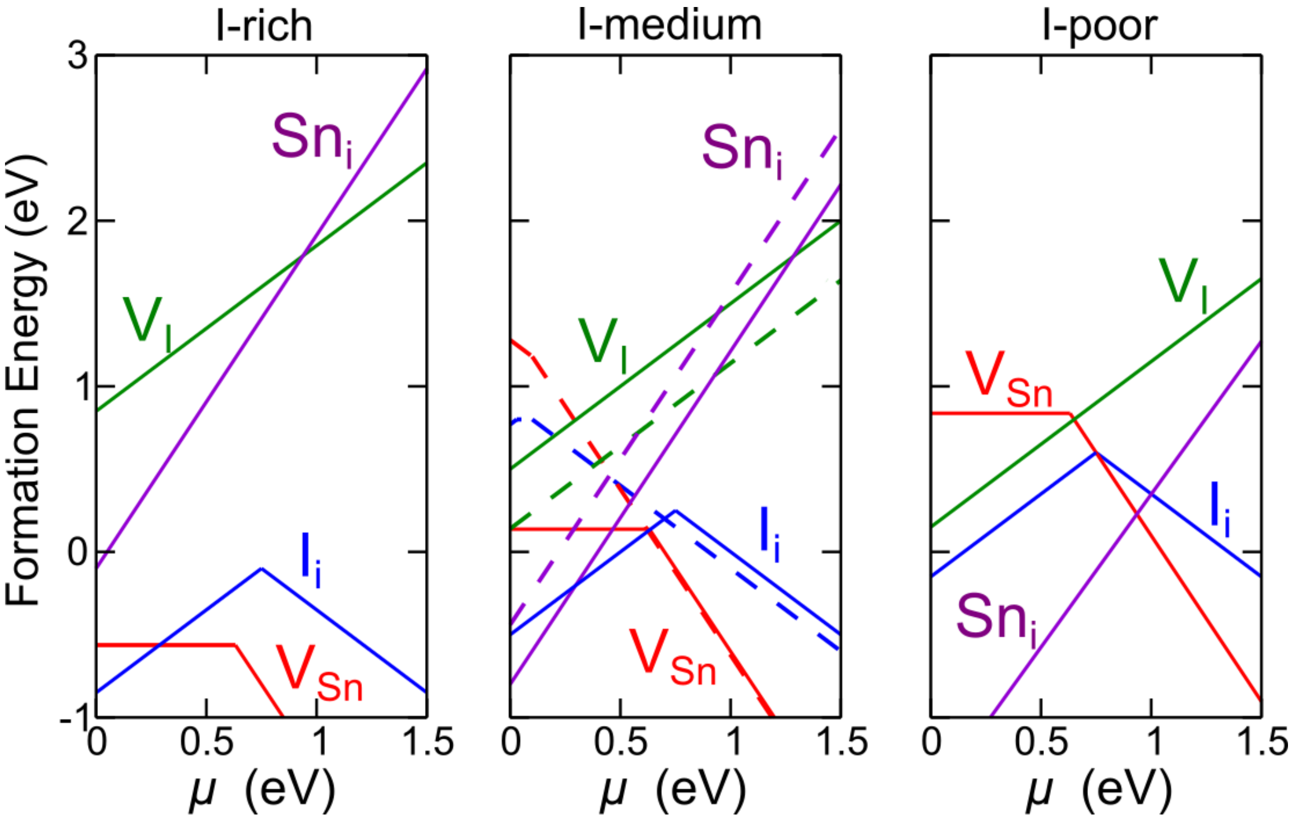

Figure 4. Formation energies of point defects on the (001) surface 1 model of $MAPb_{0.5}Sn_{0.5}I_3$ as a function of the electron chemical potential μ at different conditions. Dashed lines for the respective values calculated in the bulk material. We consider the chemical potential of Sn and I, employed in Ref. [45]: I-rich ($\mu_{Sn} = -1.39$ eV, $\mu_I = -0.16$ eV), I-medium ($\mu_{Sn} = -0.70$ eV, $\mu_I = -0.51$ eV), I-poor ($\mu_{Sn} = 0.00$ eV, $\mu_I = -0.86$ eV).

Therefore, we investigate the formation energies and charge transition levels of surface V_{Sn} and I_i at varying conditions: I-rich, I-medium and I-poor.[45] We also consider possible electron-trapping defects such as the Sn interstitial Sn_i and the iodine vacancy V_I. The formation energies of each defect as a function of the electron chemical potential (the Fermi level of the perovskite) are illustrated in Fig. 4. We first comment on the difference between bulk and surface energy levels in iodine medium conditions (middle panel of Fig. 4), corresponding to stoichiometric growth conditions. For both Sn vacancy and I interstitial we observe a remarkable difference between bulk and surface. In fact, while bulk defects feature only shallow energy levels, deep traps are observed on the surface. In particular, for V_{Sn}, we calculate the $(0/2)$ transition level at 0.63 eV above the valence band of the material. For I_i, we find the $(+1/-1)$ transition level at 0.75 eV above the valence band. These values originate from the large stabilization of surface V_{Sn}^0 and I_i^+, due to the occurrence of Sn(IV) and the tri-iodide, respectively.

Next, we analyse how different conditions influence the defects formed on the surface. First, we note that this issue is not particularly relevant for the bulk material, since it is devoid of in-gap energy levels (cf. middle panel of Fig.4). Growth conditions are more important for the surface properties. At I-rich conditions (cf. left panel of Fig. 4), V_{Sn} and I_i are found to be among the most stable defects throughout the band gap of the material. In stark contrast, hole-trapping defects are pushed towards higher formation energies at I-poor (*i.e.* Sn-rich, right panel of Fig. 4) conditions. Furthermore, we predict a higher concentration of Sn_i defects under such conditions. This defect, however, is actually harmless for the opto-electronic properties of the material, since it features charge transition levels above the conduction band edge (cf. Supplementary Information) differently from what has been observed for $MASnI_3$.[45] In view of these results, we interpret the beneficial impact of the inclusion of excess Sn powder in the precursor solution, recently demonstrated by experiments,[48] as a consequence of the higher formation energies of hole-trapping surface defects under Sn-rich conditions.

Formation energies of I_i are lower than those pertinent to V_{Sn} in a wide range of chemical and electron potentials. This, in conjunction with the impervious pathway calculated for tin oxidation on the pristine surface, corroborate the prediction that surface Sn(IV) is not easily formed in $MAPb_{0.5}Sn_{0.5}I_3$ even considering the extreme case of a fully unpassivated surface. This explains the higher long-term stability observed for mixed perovskites compared to pure THPs. Nevertheless, iodine chemistry can still induce hole-trapping with a detrimental effect on the efficiency of the associated devices.[8,47,48] We thus specifically investigate an iodine-mediated degradation pathway typically observed for LHPs,[75-77] leading to release of gaseous I_2 from I_i^+:

$$I_i^+ \rightarrow I_2(g) + V_I^+. \tag{5}$$

We calculate that reaction (5) is energetically unfavorable by ~2.3 eV (recall that I_i^+ is actually an I_3^- moiety) a value significantly higher than that previously calculated for $MAPbI_3$ (~0.9 eV).[56] While in LHPs the unfavourable energetics for I_2 release was found to be compensated by the energy gain due to the of I_3^- formation[56] this does not hold for $MAPb_{0.5}Sn_{0.5}I_3$. In fact, localization of two holes on I_3^- produce a stabilization of 0.82 eV, which is not sufficient to induce the release of molecular iodine in this case. Since I_3^- formation entails an energy gain of ~0.8-0.9 eV for both $MAPbI_3$[48] and $MAPb_{0.5}Sn_{0.5}I_3$, the remarkable difference in the energetics of the iodine release reaction is here ascribed to the higher formation energy of both bulk and surface V_I^+ for the mixed perovskite (cf. Ref. 36 and Fig. 4).The present result can explain the beneficial effect of alloying in increasing the stability of perovskite-based devices.[38-40]

Surprisingly, a significant rise in non-radiative charge recombination was reported when alloying the lead perovskite with low tin content (<20%), which suggests a different physics of charge carriers under these conditions.[63] To investigate the origin of such a puzzling behaviour we investigate hole-trapping on a PbI_2-terminated slab of tetragonal $MAPbI_3$ in which we substitute a single surface Pb with a Sn atom. Addition of a first hole on this system results in the formation of the Sn(IV) precursor, which then evolves to Sn(IV) upon capture of a second hole, with structural modifications analogous to those previously described for the mixed perovskite (cf. Fig. 2). A similar behaviour has been reported by some of us also in Sn-doped bulk $MAPbI_3$, where hole self-trapping at substitutional tin is observed for small incorporation of the dopant in the Pb site.[67]

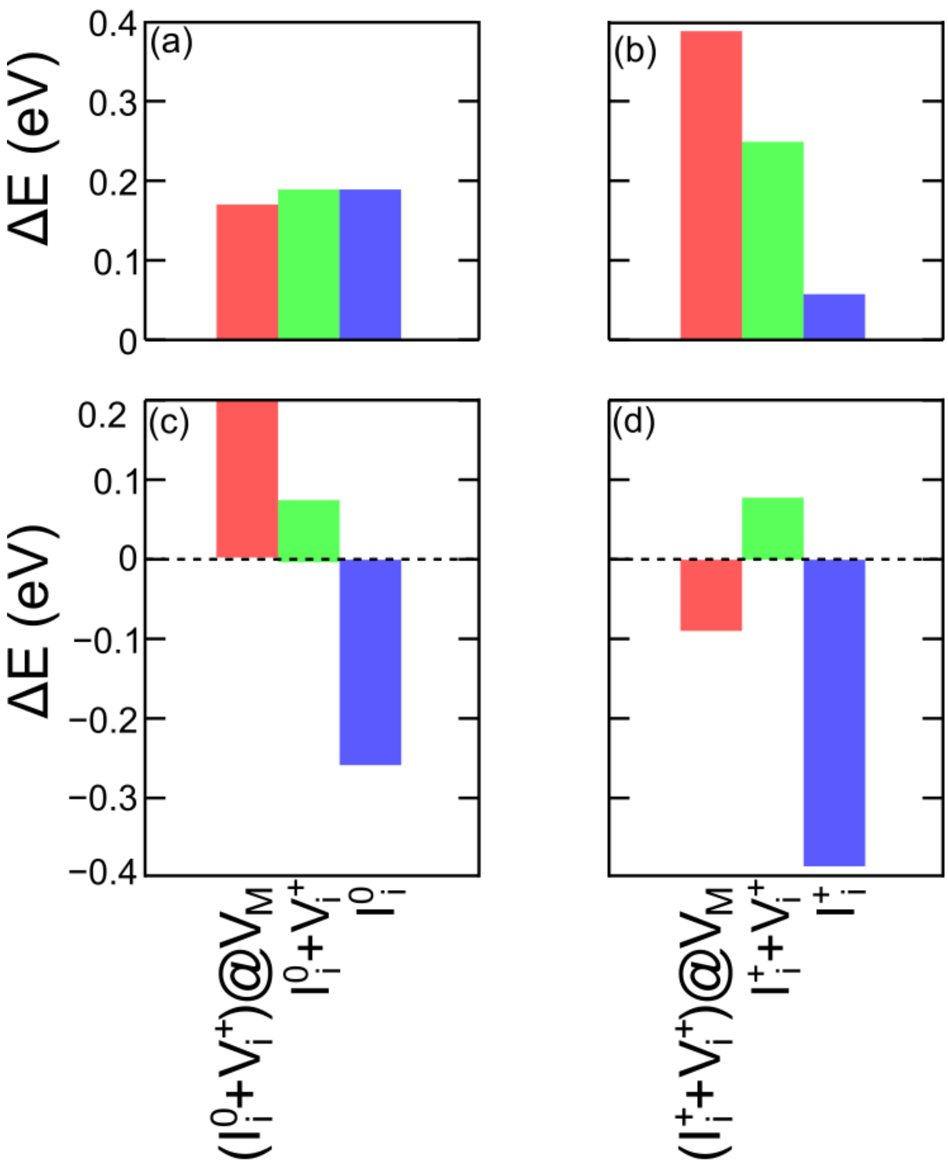

Figure 5. Energy difference (eV) between iodine-related hole-trapping species (cf. main text for definitions) and one- (a) and two-hole (b) oxidized tin moieties (cf. insets in both panels for structures and isodensity representations of holes) on pristine and defective models of the Sn-doped (001) PbI$_2$-terminated surface of MAPbI$_3$.Values achieved for pristine and defective models of the (001) surface of MAPb$_{0.5}$Sn$_{0.5}$I$_3$ are reported in panels (c) and (d) for comparison.

Hole-trapping on the pristine surface of MAPbI$_3$ is tuned by iodine chemistry, with V- and H-centers (IFDs and tri-iodide moieties) being responsible for the trapping of one (two) hole(s) on pristine and defective surfaces.[55, 56] Therefore, we compare the energetics of the Sn(IV) precursor with that of a I_2^- (either V or H-center) for the Sn-doped slab and for slabs which additionally feature a surface Pb vacancy or a I interstitial. Analogously, we investigate the energetics of surface Sn(IV) in comparison with that of IFDs and tri-iodides on pristine and defective models. The results illustrated in Fig. 5 (a) show that the Sn(IV) precursor surface trap is more stable by ~0.2 eV in all the considered cases, a result which implies a clear pathway towards tin oxidation. Concerning the trapping of two holes [cf. Fig. 5(b)], we observe that Sn(IV) is favoured over IFD formation by 0.25 eV for the pristine slab. Such an energy difference is increased (decreased) to 0.40 (0.05) eV when considering iodine defects associated with V_{Pb} (I_i). Therefore, the impact of defects on the Sn-doped $MAPbI_3$ perovskite is close to that encountered for $MAPb_{0.5}Sn_{0.5}I_{3,}$ with tin oxidation being enhanced (disfavoured) by metal vacancy (iodine interstitial). However, for the Sn-doped surface, we pinpoint that, differently from $MAPb_{0.5}Sn_{0.5}I_3$ [cf. Fig. 5 (c-d)], Sn(IV) and its precursor are found to be the most stable moieties for all the investigated systems, an instance extending the range of conditions under which tin oxidation occurs.

To summarize, we discovered a peculiar competition between tin and iodine chemistry in determining the electronic properties at the surface of mixed tin/lead perovskites. In-depth investigation of $MAPb_{0.5}Sn_{0.5}I_3$ has revealed that formation of surface Sn(IV), a harsh drawback of tin halide perovskites, competes with that of the tri-iodide, the former being favoured only in the presence of Sn vacancies. The formation of these defects in turn can be avoided by appropriately tailoring the growth conditions of the perovskite. Such a struggle, hindering the oxidation of surface Sn which undermines the stability tin-iodide perovskites, has also beneficial effects on the long-term stability of the system. In contrast, strong hole-trapping associated with surface Sn(IV) on both pristine and defective surfaces $MAPbI_3$ doped with low content of Sn was found to be related the poor electronic properties measured for perovskites incorporating only a low fraction of tin. By providing the background carrier localization pathways and associated defect chemistry, we hope this work will allow to further extend the uptake of lead-alleviated mixed tin/lead perovskites bringing them to comparable efficiency to that of pure lead perovskites.

Associated content

Supporting Information: Computational details, grand-canonical formulation of defects in periodic supercells, details of the employed structural model, analysis of hole-trapping in bulk models of $MAPb_{0.5}Sn_{0.5}I_3$, on surface 2 and 3 models and on models with modified Sn distributions on the surface, schematic representation of hole trapping mechanism on slabs bearing a Sn vacancy and a I interstitial, analysis of electron traps on surface 1 model of $MAPb_{0.5}Sn_{0.5}I_3$, and additional Refs. 78-99.

Acknowledgment:

This work was funded by the Researchers Supporting Project Number (RSP-2020/273) King Saud University, Riyadh, Saudi Arabia. This work was also supported by the European Union's Horizon 2020 research and innovation programme under grant agreement No 764047 of the ESPRESSO project. The Ministero dell'Istruzione dell'Università e della Ricerca (MIUR) and Università degli Studi di Perugia are acknowledged for financial support through the program "Dipartimenti di Eccellenza 2018-2022" (Grant AMIS) to F.D.A.

References

1. Kojima, A.; Teshima, K.; Shirai, Y.; Miyasaka, T., Organometal Halide Perovskites as Visible-Light Sensitizers for Photovoltaic Cells. *J. Am. Chem. Soc.* **2009,** *131* (17), 6050-6051.

2. Lee, M. M.; Teuscher, J.; Miyasaka, T.; Murakami, T. N.; Snaith, H. J., Efficient Hybrid Solar Cells Based on Meso-Superstructured Organometal Halide Perovskites. *Science* **2012,** *338* (6107), 643.

3. Kim, H.-S.; Lee, C.-R.; Im, J.-H.; Lee, K.-B.; Moehl, T.; Marchioro, A.; Moon, S.-J.; Humphry-Baker, R.; Yum, J.-H.; Moser, J. E.; Grätzel, M.; Park, N.-G., Lead Iodide Perovskite

Sensitized All-Solid-State Submicron Thin Film Mesoscopic Solar Cell with Efficiency Exceeding 9%. *Sci. Rep.* **2012,** *2* (1), 591.

4. Etgar, L.; Gao, P.; Xue, Z.; Peng, Q.; Chandiran, A. K.; Liu, B.; Nazeeruddin, M. K.; Grätzel, M., Mesoscopic $CH_3NH_3PbI_3/TiO_2$ Heterojunction Solar Cells. *J. Am. Chem. Soc.* **2012,** *134* (42), 17396-17399.

5. Burschka, J.; Pellet, N.; Moon, S.-J.; Humphry-Baker, R.; Gao, P.; Nazeeruddin, M. K.; Grätzel, M., Sequential Deposition as a Route to High-Performance Perovskite-Sensitized Solar Cells. *Nature* **2013,** *499*, 316.

6. Brenner, T. M.; Egger, D. A.; Kronik, L.; Hodes, G.; Cahen, D., Hybrid Organic—Inorganic Perovskites: Low-Cost Semiconductors with Intriguing Charge-Transport Properties. *Nat. Rev. Mater.* **2016,** *1*, 15007.

7. Meggiolaro, D.; Ambrosio, F.; Mosconi, E.; Mahata, A.; De Angelis, F., Polarons in Metal Halide Perovskites. *Adv. Energy Mater.* **2019,** *n/a* (n/a), 1902748.

8. https://www.nrel.gov/pv/assets/images/efficiency-chart.png (accessed on 13 September 2019).

9. Ponseca, C. S.; Savenije, T. J.; Abdellah, M.; Zheng, K.; Yartsev, A.; Pascher, T.; Harlang, T.; Chabera, P.; Pullerits, T.; Stepanov, A.; Wolf, J.-P.; Sundström, V., Organometal Halide Perovskite Solar Cell Materials Rationalized: Ultrafast Charge Generation, High and Microsecond-Long Balanced Mobilities, and Slow Recombination. *J. Am. Chem. Soc.* **2014,** *136* (14), 5189-5192.

10. Edri, E., E. Edri, S. Kirmayer, S. Mukhopadhyay, K. Gartsman, G. Hodes, and D. Cahen, Elucidating the Charge Carrier Separation and Working Mechanism of $CH_3NH_3PbI_{3-x}Cl_x$ perovskite solar cells, *Nat. Commun.* **2014,** *5*, 3461.

11. Hutter, E. M.; Gélvez-Rueda, M. C.; Osherov, A.; Bulović, V.; Grozema, F. C.; Stranks, S. D.; Savenije, T. J., Direct–Indirect Character of the Bandgap in Methylammonium Lead Iodide Perovskite. *Nat. Mater.* **2016,** *16*, 115.

12. Crothers, T. W.; Milot, R. L.; Patel, J. B.; Parrott, E. S.; Schlipf, J.; Müller-Buschbaum, P.; Johnston, M. B.; Herz, L. M., Photon Reabsorption Masks Intrinsic Bimolecular Charge-Carrier Recombination in $CH_3NH_3PbI_3$ Perovskite. *Nano Lett.* **2017,** *17* (9), 5782-5789.

13. Stranks, S. D.; Eperon, G. E.; Grancini, G.; Menelaou, C.; Alcocer, M. J. P.; Leijtens, T.; Herz, L. M.; Petrozza, A.; Snaith, H. J., Electron-Hole Diffusion Lengths Exceeding 1 Micrometer in an Organometal Trihalide Perovskite Absorber. *Science* **2013,** *342* (6156), 341-344.

14. Ambrosio, F.; Wiktor, J.; De Angelis, F.; Pasquarello, A., Origin of Low Electron–Hole Recombination Rate in Metal Halide Perovskites. *Energy Environ. Sci.* **2018,** *11* (1), 101-105.

15. Ambrosio, F.; Meggiolaro, D.; Mosconi, E.; De Angelis, F., Charge Localization, Stabilization, and Hopping in Lead Halide Perovskites: Competition between Polaron Stabilization and Cation Disorder. *ACS Energy Lett.* **2019,** *4* (8), 2013-2020.

16. Motti, S. G.; Meggiolaro, D.; Martani, S.; Sorrentino, R.; Barker, A. J.; De Angelis, F.; Petrozza, A., Defect Activity in Metal–Halide Perovskites. *Adv. Mater.* **2019,** *0* (0), 1901183.

17. Kim, J.; Lee, S.-H.; Lee, J. H.; Hong, K.-H., The Role of Intrinsic Defects in Methylammonium Lead Iodide Perovskite. *J. Phys. Chem. Lett.* **2014,** *5* (8), 1312-1317.

18. Yamada, Y.; Endo, M.; Wakamiya, A.; Kanemitsu, Y., Spontaneous Defect Annihilation in CH3NH3PbI3 Thin Films at Room Temperature Revealed by Time-Resolved Photoluminescence Spectroscopy. *J. Phys. Chem. Lett.* **2015,** *6* (3), 482-486.

19. Buin, A.; Pietsch, P.; Xu, J.; Voznyy, O.; Ip, A. H.; Comin, R.; Sargent, E. H., Materials Processing Routes to Trap-Free Halide Perovskites. *Nano Lett.* **2014,** *14* (11), 6281-6286.

20. Dagnall, K. A.; Foley, B. J.; Cuthriell, S. A.; Alpert, M. R.; Deng, X.; Chen, A. Z.; Sun, Z.; Gupta, M. C.; Xiao, K.; Lee, S.-H.; Ma, Y.-Z.; Choi, J. J., Relationship between the Nature of Monovalent Cations and Charge Recombination in Metal Halide Perovskites. *ACS Appl. Energy Mater*. **2020**.

21. Meggiolaro, D.; Motti, S. G.; Mosconi, E.; Barker, A. J.; Ball, J.; Andrea Riccardo Perini, C.; Deschler, F.; Petrozza, A.; De Angelis, F., Iodine Chemistry Determines the Defect Tolerance of Lead-Halide Perovskites. *Energy Environ. Sci.* **2018,** *11* (3), 702-713.

22. Chu, W.; Zheng, Q.; Prezhdo, O. V.; Zhao, J.; Saidi, W. A., Low-Frequency Lattice Phonons in Halide Perovskites Explain High Defect Tolerance Toward Electron-Hole Recombination. *Sci. Adv.* **2020,** *6* (7).

23. Chu, W.; Saidi, W. A.; Zhao, J.; Prezhdo, O. V., Soft Lattice and Defect Covalency Rationalize Tolerance of β-$CsPbI_3$ Perovskite Solar Cells to Native Defects. *Angew. Chem.* **2020,** *59* (16), 6435-6441.

24. Babayigit, A.; Ethirajan, A.; Muller, M.; Conings, B., Toxicity of Organometal Halide Perovskite Solar Cells. *Nat. Mater.* **2016,** *15* (3), 247-251.

25. Li, J.; Cao, H.-L.; Jiao, W.-B.; Wang, Q.; Wei, M.; Cantone, I.; Lü, J.; Abate, A., Biological Impact of Lead from Halide Perovskites Reveals the Risk of Introducing a Safe Threshold. *Nat. Commun.* **2020,** *11* (1), 310.

26. Park, S. Y.; Park, J.-S.; Kim, B. J.; Lee, H.; Walsh, A.; Zhu, K.; Kim, D. H.; Jung, H. S., Sustainable Lead Management in Halide Perovskite Solar Cells. *Nat. Sustain.* **2020**.

27. Zhang, Y.; Park, N.-G., A Thin Film (<200 nm) Perovskite Solar Cell with 18% Efficiency. *.J Mater. Chem. A* **2020,** *8* (34), 17420-17428.

28. Zhang, F.; Lu, H.; Tong, J.; Berry, J. J.; Beard, M. C.; Zhu, K., Advances in Two-Dimensional Organic–Inorganic Hybrid Perovskites. *Energy Environ. Sci.* **2020,** *13* (4), 1154-1186.

29. Giustino, F.; Snaith, H. J., Toward Lead-Free Perovskite Solar Cells. *ACS Energy Lett.* **2016,** *1* (6), 1233-1240.

30. Noel, N. K.; Stranks, S. D.; Abate, A.; Wehrenfennig, C.; Guarnera, S.; Haghighirad, A.-A.; Sadhanala, A.; Eperon, G. E.; Pathak, S. K.; Johnston, M. B.; Petrozza, A.; Herz, L. M.; Snaith, H. J., Lead-Free Organic–Inorganic Tin Halide Perovskites for Photovoltaic Applications. *Energy Environ. Sci.* **2014,** *7* (9), 3061-3068.

31. Konstantakou, M.; Stergiopoulos, T., A Critical Review on Tin Halide Perovskite Solar Cells. *.J Mater. Chem. A* **2017,** *5* (23), 11518-11549.

32. Stoumpos, C. C.; Frazer, L.; Clark, D. J.; Kim, Y. S.; Rhim, S. H.; Freeman, A. J.; Ketterson, J. B.; Jang, J. I.; Kanatzidis, M. G., Hybrid Germanium Iodide Perovskite Semiconductors: Active Lone Pairs, Structural Distortions, Direct and Indirect Energy Gaps, and Strong Nonlinear Optical Properties. *J. Am. Chem. Soc.* **2015,** *137* (21), 6804-6819.

33. McClure, E. T.; Ball, M. R.; Windl, W.; Woodward, P. M., Cs_2AgBiX_6 (X = Br, Cl): New Visible Light Absorbing, Lead-Free Halide Perovskite Semiconductors. *Chem. Mater.* **2016,** *28* (5), 1348-1354.

34. Filip, M. R.; Hillman, S.; Haghighirad, A. A.; Snaith, H. J.; Giustino, F., Band Gaps of the Lead-Free Halide Double Perovskites $Cs_2BiAgCl_6$ and $Cs_2BiAgBr_6$ from Theory and Experiment. *J. Phys. Chem. Lett.* **2016,** *7* (13), 2579-2585.

35. Slavney, A. H.; Hu, T.; Lindenberg, A. M.; Karunadasa, H. I., A Bismuth-Halide Double Perovskite with Long Carrier Recombination Lifetime for Photovoltaic Applications. *J. Am. Chem. Soc.* **2016,** *138* (7), 2138-2141.

36. Hao, F.; Stoumpos, C. C.; Cao, D. H.; Chang, R. P. H.; Kanatzidis, M. G., Lead-free Solid-state Organic–inorganic Halide Perovskite oslar Cells. *Nat. Photonics* **2014,** *8* (6), 489-494.

37. Umari, P.; Mosconi, E.; De Angelis, F., Relativistic GW Calculations on $CH_3NH_3PbI_3$ and $CH_3NH_3SnI_3$ Perovskites for Solar Cell Applications. *Sci. Rep.* **2014,** *4*, 4467.

38. Mosconi, E.; Umari, P.; De Angelis, F., Electronic and Optical Properties of Mixed Sn–Pb Organohalide Perovskites: A First Principles Investigation. *J. Mater. Chem. A* **2015,** *3* (17), 9208-9215.

39. Kumar, M. H.; Dharani, S.; Leong, W. L.; Boix, P. P.; Prabhakar, R. R.; Baikie, T.; Shi, C.; Ding, H.; Ramesh, R.; Asta, M.; Graetzel, M.; Mhaisalkar, S. G.; Mathews, N., Lead-Free Halide Perovskite Solar Cells with High Photocurrents Realized Through Vacancy Modulation. *Adv. Mater.* **2014,** *26* (41), 7122-7127.

40. Xiao, Z.; Song, Z.; Yan, Y., From Lead Halide Perovskites to Lead-Free Metal Halide Perovskites and Perovskite Derivatives. *Adv. Mater.* **2019,** *31* (47), 1803792.

41. Nishimura, K.; Kamarudin, M. A.; Hirotani, D.; Hamada, K.; Shen, Q.; Iikubo, S.; Minemoto, T.; Yoshino, K.; Hayase, S., Lead-free Tin-halide Perovskite Solar cells with 13% Efficiency. *Nano Energy* **2020,** *74*, 104858.

42. Dalpian, G. M.; Liu, Q.; Stoumpos, C. C.; Douvalis, A. P.; Balasubramanian, M.; Kanatzidis, M. G.; Zunger, A., Changes in Charge Density vs Changes in Formal Oxidation States: The Case of Sn Halide Perovskites and their Ordered Vacancy Analogues. *Phys. Rev. Mater.* **2017,** *1* (2), 025401.

43. Bowman, A. R.; Klug, M. T.; Doherty, T. A. S.; Farrar, M. D.; Senanayak, S. P.; Wenger, B.; Divitini, G.; Booker, E. P.; Andaji-Garmaroudi, Z.; Macpherson, S.; Ruggeri, E.; Sirringhaus, H.; Snaith, H. J.; Stranks, S. D., Microsecond Carrier Lifetimes, Controlled p-Doping, and Enhanced Air Stability in Low-Bandgap Metal Halide Perovskites. *ACS Energy Lett.* **2019,** *4* (9), 2301-2307.

44. Milot, R. L.; Klug, M. T.; Davies, C. L.; Wang, Z.; Kraus, H.; Snaith, H. J.; Johnston, M. B.; Herz, L. M., The Effects of Doping Density and Temperature on the Optoelectronic Properties of Formamidinium Tin Triiodide Thin Films. *Adv. Mater.* **2018,** *30* (44), 1804506.

45. Meggiolaro, D.; Ricciarelli, D.; Alasmari, A. A.; Alasmary, F. A. S.; De Angelis, F., Tin versus Lead Redox Chemistry Modulates Charge Trapping and Self-Doping in Tin/Lead Iodide Perovskites. *J. Phys. Chem. Lett.* **2020,** *11* (9), 3546-3556.

46. Ricciarelli, D.; Meggiolaro, D.; Ambrosio, F.; De Angelis, F., Instability of Tin Iodide Perovskites: Bulk p-doping vs. Surface Tin Oxidation. *ACS Energy Lett.* **2020**.

47. Zhao, D.; Yu, Y.; Wang, C.; Liao, W.; Shrestha, N.; Grice, C. R.; Cimaroli, A. J.; Guan, L.; Ellingson, R. J.; Zhu, K.; Zhao, X.; Xiong, R.-G.; Yan, Y., Low-bandgap Mixed Tin–lead Iodide Perovskite Absorbers with Long Carrier Lifetimes for all-Perovskite Tandem Solar Cells. *Nat. Energy* **2017,** *2* (4), 17018.

48. Jiang, T.; Chen, Z.; Chen, X.; Liu, T.; Chen, X.; Sha, W. E. I.; Zhu, H.; Yang, Y., Realizing High Efficiency over 20% of Low-Bandgap Pb–Sn-Alloyed Perovskite Solar Cells by In Situ Reduction of Sn4+. *Solar RRL* **2020,** *4* (3), 1900467.

49. Li, C.; Song, Z.; Chen, C.; Xiao, C.; Subedi, B.; Harvey, S. P.; Shrestha, N.; Subedi, K. K.; Chen, L.; Liu, D.; Li, Y.; Kim, Y.-W.; Jiang, C.-s.; Heben, M. J.; Zhao, D.; Ellingson, R. J.; Podraza, N. J.; Al-Jassim, M.; Yan, Y., Low-bandgap Mixed Tin–lead Iodide perovskites with Reduced Methylammonium for Simultaneous Enhancement of Solar Cell Efficiency and Stability. *Nat. Energy* **2020,** *5* (10), 768-776.

50. Hao, F.; Stoumpos, C. C.; Chang, R. P. H.; Kanatzidis, M. G., Anomalous Band Gap Behavior in Mixed Sn and Pb Perovskites Enables Broadening of Absorption Spectrum in Solar Cells. *J. Am. Chem. Soc.* **2014,** *136* (22), 8094-8099.

51. Wiktor, J.; Ambrosio, F.; Pasquarello, A., Mechanism Suppressing Charge Recombination at Iodine Defects in $CH_3NH_3PbI_3$ by Polaron Formation. *J. Mater. Chem. A* **2018,** *6* (35), 16863-16867.

52. Schulz, P.; Cahen, D.; Kahn, A., Halide Perovskites: Is It All about the Interfaces? *Chem. Rev.* **2019,** *119* (5), 3349-3417.

53. Ono, L. K.; Qi, Y., Surface and Interface Aspects of Organometal Halide Perovskite Materials and Solar Cells. *J. Phys. Chem. Lett.* **2016,** *7* (22), 4764-4794.

54. Wu, B.; Nguyen, H. T.; Ku, Z.; Han, G.; Giovanni, D.; Mathews, N.; Fan, H. J.; Sum, T. C., Discerning the Surface and Bulk Recombination Kinetics of Organic–Inorganic Halide Perovskite Single Crystals. *Adv. Energy Mater.* **2016,** *6* (14), 1600551.

55. Ambrosio, F.; Meggiolaro, D.; Mosconi, E.; De Angelis, F., Charge Localization and Trapping at Surfaces in Lead-Iodide Perovskites: The Role of Polarons and Defects. *J. Mater. Chem. A* **2020,** *8* (14), 6882-6892.

56. Ambrosio, F.; Mosconi, E.; Alasmari, A. A.; Alasmary, F. A. S.; Meggiolaro, D.; De Angelis, F., Formation of Colour Centres in Lead-Iodide Perovskites: Self-trapping and Defects in Bulk and Surfaces. *Chem. Mater.* **2020**.

57. Yang, Y.; Yang, M.; Moore, David T.; Yan, Y.; Miller, Elisa M.; Zhu, K.; Beard, Matthew C., Top and Bottom Surfaces Limit Carrier Lifetime in Lead Iodide Perovskite Films. *Nat. Energy* **2017,** *2*, 16207.

58. Xu, J.; Buin, A.; Ip, A. H.; Li, W.; Voznyy, O.; Comin, R.; Yuan, M.; Jeon, S.; Ning, Z.; McDowell, J. J.; Kanjanaboos, P.; Sun, J.-P.; Lan, X.; Quan, L. N.; Kim, D. H.; Hill, I. G.; Maksymovych, P.; Sargent, E. H., Perovskite–fullerene hybrid materials suppress hysteresis in planar diodes. *Nat. Commun.* **2015,** *6*, 7081.

59. Zhang, H.; Wu, Y.; Shen, C.; Li, E.; Yan, C.; Zhang, W.; Tian, H.; Han, L.; Zhu, W.-H., Efficient and Stable Chemical Passivation on Perovskite Surface via Bidentate Anchoring. *Adv. Energy Mater.* **2019,** *9* (13), 1803573.

60. Noel, N. K.; Abate, A.; Stranks, S. D.; Parrott, E. S.; Burlakov, V. M.; Goriely, A.; Snaith, H. J., Enhanced Photoluminescence and Solar Cell Performance via Lewis Base Passivation of Organic–Inorganic Lead Halide Perovskites. *ACS Nano* **2014,** *8* (10), 9815-9821.

61. Yang, S.; Dai, J.; Yu, Z.; Shao, Y.; Zhou, Y.; Xiao, X.; Zeng, X. C.; Huang, J., Tailoring Passivation Molecular Structures for Extremely Small Open-Circuit Voltage Loss in Perovskite Solar Cells. *J. Am. Chem. Soc.* **2019,** *141* (14), 5781-5787.

62. Wang, Q.; Mosconi, E.; Wolff, C.; Li, J.; Neher, D.; De Angelis, F.; Suranna, G. P.; Grisorio, R.; Abate, A., Rationalizing the Molecular Design of Hole-Selective Contacts to Improve Charge Extraction in Perovskite Solar Cells. *Adv. Energy Mater.* **2019,** *9* (28), 1900990.

63. Klug, M. T.; Milot, R. L.; Patel, J. B.; Green, T.; Sansom, H. C.; Farrar, M. D.; Ramadan, A. J.; Martani, S.; Wang, Z.; Wenger, B.; Ball, J. M.; Langshaw, L.; Petrozza, A.; Johnston, M. B.; Herz, L. M.; Snaith, H. J., Metal composition influences optoelectronic quality in mixed-metal lead–tin triiodide perovskite solar absorbers. *Energy Environ. Sci.* **2020,** *13* (6), 1776-1787.

64. Abdollahi Nejand, B.; Hossain, I. M.; Jakoby, M.; Moghadamzadeh, S.; Abzieher, T.; Gharibzadeh, S.; Schwenzer, J. A.; Nazari, P.; Schackmar, F.; Hauschild, D.; Weinhardt, L.; Lemmer, U.; Richards, B. S.; Howard, I. A.; Paetzold, U. W., Vacuum-Assisted Growth of Low-

Bandgap Thin Films (FA0.8MA0.2Sn0.5Pb0.5I3) for All-Perovskite Tandem Solar Cells. *Adv. Energy Mater.* **2020,** *10* (5), 1902583.

65. Liu, M.; Chen, Z.; Xue, Q.; Cheung, S. H.; So, S. K.; Yip, H.-L.; Cao, Y., High performance low-bandgap perovskite solar cells based on a high-quality mixed Sn–Pb perovskite film prepared by vacuum-assisted thermal annealing. *J. Mater. Chem. A* **2018,** *6* (34), 16347-16354.

66. Tong, J.; Song, Z.; Kim, D. H.; Chen, X.; Chen, C.; Palmstrom, A. F.; Ndione, P. F.; Reese, M. O.; Dunfield, S. P.; Reid, O. G., Carrier lifetimes of> 1 μs in Sn-Pb perovskites enable efficient all-perovskite tandem solar cells. *Science* **2019,** *364* (6439), 475-479.

67. Mahata, A.; Meggiolaro, D.; De Angelis, F., From Large to Small Polarons in Lead, Tin, and Mixed Lead–Tin Halide Perovskites. *J. Phys. Chem. Lett.* **2019,** *10* (8), 1790-1798.

68. Popov, A. I.; Kotomin, E. A.; Maier, J., Analysis of self-trapped hole mobility in alkali halides and metal halides. *Solid State Ion.* **2017,** *302*, 3-6.

69. Sonder, E.; Sibley, W. A., Point defects in solids. *Ed. JH CRAWFORD, Jr. and LM SLIFKIN* **1972**.

70. Williams, R. T.; Song, K. S., The self-trapped exciton. *J. Phys. Chem. Solids* **1990,** *51* (7), 679-716.

71. Stoneham, A. M., *Theory of defects in solids: electronic structure of defects in insulators and semiconductors*. Oxford University Press: 2001.

72. Halgren, T. A.; Lipscomb, W. N., The synchronous-transit method for determining reaction pathways and locating molecular transition states. *Chem. Phys. Lett.* **1977,** *49* (2), 225-232.

73. Kim, S. H.; Lee, D., Role of Charge-Trapping Iodine Frenkel Defects for Hysteresis in Organic–Inorganic Hybrid Perovskite from First-Principles Calculations. *J. Phys. Chem. C* **2019,** *123* (14), 9629-9633.

74. Meggiolaro, D.; De Angelis, F., First-Principles Modeling of Defects in Lead Halide Perovskites: Best Practices and Open Issues. *ACS Energy Lett.* **2018,** *3* (9), 2206-2222.

75. Motti, S. G.; Meggiolaro, D.; Barker, A. J.; Mosconi, E.; Perini, C. A. R.; Ball, J. M.; Gandini, M.; Kim, M.; De Angelis, F.; Petrozza, A., Controlling competing photochemical reactions stabilizes perovskite solar cells. *Nat. Photonics* **2019,** *13* (8), 532-539.

76. Kim, G. Y.; Senocrate, A.; Yang, T.-Y.; Gregori, G.; Grätzel, M.; Maier, J., Large tunable photoeffect on ion conduction in halide perovskites and implications for photodecomposition. *Nature materials* **2018,** *17* (5), 445-449.

77. Samu, G. F.; Balog, Á.; De Angelis, F.; Meggiolaro, D.; Kamat, P. V.; Janáky, C., Electrochemical Hole Injection Selectively Expels Iodide from Mixed Halide Perovskite Films. *J. Am. Chem. Soc.* **2019,** *141* (27), 10812-10820.

78. Perdew, J. P.; Ernzerhof, M.; Burke, K., Rationale for mixing exact exchange with density functional approximations. *J. Chem. phys.* **1996,** *105* (22), 9982-9985.

79. Adamo, C.; Barone, V., Toward reliable density functional methods without adjustable parameters: The PBE0 model. *J. Chem. phys.* **1999,** *110* (13), 6158-6170.

80. Vydrov, O. A.; Van Voorhis, T., Nonlocal van der Waals density functional: The simpler the better. *J. Chem. phys.* **2010,** *133* (24), 244103.

81. Sabatini, R.; Gorni, T.; De Gironcoli, S., Nonlocal van der Waals density functional made simple and efficient. *Phys. Rev. B* **2013,** *87* (4), 041108.

82. VandeVondele, J.; Krack, M.; Mohamed, F.; Parrinello, M.; Chassaing, T.; Hutter, J., Quickstep: Fast and accurate density functional calculations using a mixed Gaussian and plane waves approach. *Comput. Phys. Commun.* **2005,** *167* (2), 103-128.

83. Goedecker, S.; Teter, M.; Hutter, J., Separable dual-space Gaussian pseudopotentials. *Phys. Rev. B* **1996,** *54* (3), 1703.

84. VandeVondele, J.; Hutter, J., Gaussian basis sets for accurate calculations on molecular systems in gas and condensed phases. *J. Chem. phys.* **2007,** *127* (11), 114105.

85. Guidon, M.; Hutter, J.; VandeVondele, J., Auxiliary Density Matrix Methods for Hartree−Fock Exchange Calculations. *J. Chem. Theory Comput.* **2010,** *6* (8), 2348-2364.

86. Giannozzi, P.; Baroni, S.; Bonini, N.; Calandra, M.; Car, R.; Cavazzoni, C.; Ceresoli, D.; Chiarotti, G. L.; Cococcioni, M.; Dabo, I.; Dal Corso, A.; de Gironcoli, S.; Fabris, S.; Fratesi, G.; Gebauer, R.; Gerstmann, U.; Gougoussis, C.; Kokalj, A.; Lazzeri, M.; Martin-Samos, L.; Marzari, N.; Mauri, F.; Mazzarello, R.; Paolini, S.; Pasquarello, A.; Paulatto, L.; Sbraccia, C.; Scandolo, S.; Sclauzero, G.; Seitsonen, A. P.; Smogunov, A.; Umari, P.; Wentzcovitch, R. M., QUANTUM ESPRESSO: a modular and open-source software project for quantum simulations of materials. *J. Phys Condens. Matter* **2009,** *21* (39), 395502.

87. Hamann, D. R., Optimized norm-conserving Vanderbilt pseudopotentials. *Phys. Rev. B* **2013,** *88* (8), 085117.

88. Komsa, H.-P.; Rantala, T. T.; Pasquarello, A., Finite-size supercell correction schemes for charged defect calculations. *Phys. Rev. B* **2012,** *86* (4), 045112.

89. Freysoldt, C.; Grabowski, B.; Hickel, T.; Neugebauer, J.; Kresse, G.; Janotti, A.; Van de Walle, C. G., First-principles calculations for point defects in solids. *Rev. Mod. Phys.* **2014,** *86* (1), 253-305.

90. Freysoldt, C.; Neugebauer, J.; Van de Walle, C. G., Fully Ab Initio Finite-Size Corrections for Charged-Defect Supercell Calculations. *Phys. Rev. Lett.* **2009,** *102* (1), 016402.

91. Komsa, H.-P.; Pasquarello, A., Finite-Size Supercell Correction for Charged Defects at Surfaces and Interfaces. *Phys. Rev. Lett.* **2013,** *110* (9), 095505.

92. Haruyama, J.; Sodeyama, K.; Han, L.; Tateyama, Y., Termination Dependence of Tetragonal CH3NH3PbI3 Surfaces for Perovskite Solar Cells. *J. Phys. Chem. Lett.* **2014,** *5* (16), 2903-2909.

93. Haruyama, J.; Sodeyama, K.; Han, L.; Tateyama, Y., Surface Properties of CH3NH3PbI3 for Perovskite Solar Cells. *Acc. Chem. Res.* **2016,** *49* (3), 554-561.

94. Baikie, T.; Fang, Y.; Kadro, J. M.; Schreyer, M.; Wei, F.; Mhaisalkar, S. G.; Graetzel, M.; White, T. J., Synthesis and crystal chemistry of the hybrid perovskite (CH3NH3)PbI3 for solid-state sensitised solar cell applications. *J. Mater. Chem. A* **2013,** *1* (18), 5628-5641.

95. Even, J.; Pedesseau, L.; Jancu, J.-M.; Katan, C., Importance of Spin–Orbit Coupling in Hybrid Organic/Inorganic Perovskites for Photovoltaic Applications. *J. Phys. Chem. Lett.* **2013,** *4* (17), 2999-3005.

96. Im, J.; Stoumpos, C. C.; Jin, H.; Freeman, A. J.; Kanatzidis, M. G., Antagonism between Spin–Orbit Coupling and Steric Effects Causes Anomalous Band Gap Evolution in the Perovskite Photovoltaic Materials CH3NH3Sn1–xPbxI3. *J. Phys. Chem. Lett.* **2015,** *6* (17), 3503-3509.

97. Poglitsch, A.; Weber, D., Dynamic disorder in methylammoniumtrihalogenoplumbates (II) observed by millimeter-wave spectroscopy. *J. Chem. phys.***1987,** *87* (11), 6373-6378.

98. Guan, L.; Xu, X.; Liang, Y.; Han, S.; Guo, J.; Wang, J.; Li, X., Effect of atomic configuration on band gap behaviour in CH3NH3SnxPb1−xI3 perovskites. *Phys. Lett. A* **2020,** *384* (8), 126173.

99. Meggiolaro, D.; Mosconi, E.; Proppe, A. H.; Quintero-Bermudez, R.; Kelley, S. O.; Sargent, E. H.; De Angelis, F., Energy Level Tuning at the MAPbI3 Perovskite/Contact Interface Using Chemical Treatment. *ACS Energy Lett.* **2019,** *4* (9), 2181-2184.

Supplementary Information for:

Composition-Dependent Struggle Between Iodine and Tin Chemistry at the Surface of Mixed Tin/Lead Perovskites

Francesco Ambrosio,[a,b,]* Daniele Meggiolaro,[b] Tahani M. Almutairi,[d] Filippo De Angelis [a,b,c]*

[a]*CompuNet, Istituto Italiano di Tecnologia, Via Morego 30, 16163 Genova, Italy.*

[b]*Computational Laboratory for Hybrid/Organic Photovoltaics (CLHYO), Istituto CNR di Scienze e Tecnologie Chimiche "Giulio Natta" (CNR-SCITEC), Via Elce di Sotto 8, 06123 Perugia, Italy.*

[c]*Department of Chemistry, Biology and Biotechnology, University of Perugia, Via Elce di Sotto 8, 06123 Perugia, Italy.*

[d] *Chemistry Department, College of Science, King Saud University, Riyadh 11451, Saudi Arabia.*

*E-mail: Francesco.Ambrosio@iit.it, filippo@thch.unipg.it

S1. Computational details

We carry out hybrid DFT calculations at the PBE0+rVV10 level of theory[1, 2 3, 4], in line with previous publications. [5-7] We include non-local van der Waals interactions through the rVV10 scheme, in which the b parameter governing the extent of long-range interactions is set to its original value of 6.3.[3, 4] All calculations are carried out with the freely-available CP2K suite of codes.[8] Goedecker-Teter-Hutter pseudopotentials are used to account for core-valence interactions.[9] We use double-ζ polarized basis sets for the wave functions[10] and a cut-off of 600 Ry for the expansion of the electron density in plane waves. We employ the auxiliary density matrix method to speed up the calculation of exact exchange in hybrid functional calculations as implemented in CP2K with the cFIT auxiliary basis set.[11] Spin-polarized calculations are performed on systems bearing an odd number of electrons. We note that spin-orbit coupling (SOC), while significantly contributing to the electronic properties of metal halide perovskite, [12, 13] does not affect those originating from the valence band edge,[7, 14] such as hole localization and trapping mainly studied in this work. At variance with this, SOC impact principally on the electronic properties associated with conduction band edge states.[13] Therefore, we perform supplementary calculations with the QUANTUM ESPRESSO code[15] employing full relativistic pseudopotentials[16] on the structures achieved without SOC for systems in which extra electrons have been added (cf. Section S7).

Calculations of energy barriers for hole trapping on interstitial iodide are carried out using a modified version of the linear transit method[17] previously employed in Ref. 18. The coordinates of the two structures R_i and R_j are linearly interpolated[17] according to the following expression: $R_\lambda = \lambda R_i + (1-\lambda)R_j$ where λ is the coupling parameter connecting the two models. The achieved structures are then allowed to undergo structural relaxation in which the organic cations are free to relax. In contrast, the positions of the atoms belonging to the inorganic sub-lattice are fixed. In this way, we avoid unstable and highly energetic structures due to linear interpolation of the coordinates of the freely-rotating organic cations. The accuracy of this methodology has been checked in previous studies.[7, 18]

S2. Grand-canonical formulation of defects in semiconductors

To calculate the energy levels of defects, we here employ the grand-canonical formulation of defects in crystalline materials.[19, 20] This theory allows to express the formation energy of a defect X with charge q, $E_f^q[X]$ as a function of the electron chemical potential μ:

$$E_f^q[X] = E^q[X] - E[\text{ref}] - \sum_i n_i\mu_i + q(\varepsilon_\text{V} + \mu) + E_\text{corr}^q \tag{S1}$$

In Eq. S1, $E^q[X]$ is the total energy of the defect X in the charge state q, $E[\text{ref}]$ the total energy of the pristine system, μ_i the chemical potential of the subtracted/added species i, ε_V the valence band edge of the pristine system, and E_corr^q a correction term, here introduced to account for electrostatic finite-size effects of charged periodic supercells. The charge transition level $\mu(q/q')$ is defined as the electron chemical potential for which the formation energies of a defect X in the charge states q and q' are equal ($E_f^q[X] = E_f^{q'}[X]$):

$$\mu(q/q') = \frac{E^q[X] - E^{q'}[X]}{q' - q} + \frac{E_{corr}^q - E_{corr}^{q'}}{q' - q} - \varepsilon_\text{V}. \tag{S2}$$

The binding energies of hole and electron polarons in mixed perovskites are calculated considering the following reactions, respectively:

$$\text{MAPb}_{1-\text{x}}\text{Sn}_\text{x}\text{I}_3 + h^+ \longrightarrow h_\text{loc}, \tag{S3}$$

$$\text{MAPb}_{1-\text{x}}\text{Sn}_\text{x}\text{I}_3 + e^- \longrightarrow e_\text{loc}, \tag{S4}$$

From. Eq. S2, the hole and electron polaron levels are defined as follows, respectively:

$$\mu(h_\text{loc}) = -E[h_\text{loc}] + E[\text{MAPb}_{1-\text{x}}\text{Sn}_\text{x}\text{I}_3] - E_{corr}^{+1} - \varepsilon_\text{V}, \tag{S5}$$

$$\mu(e_\text{loc}) = E[e_\text{loc}] - E[\text{MAPb}_{1-\text{x}}\text{Sn}_\text{x}\text{I}_3] + E_{corr}^{-1} - \varepsilon_\text{V}, \tag{S6}$$

where $E[h_{\mathrm{loc}}]$ and $E[e_{\mathrm{loc}}]$ are the total energies of the supercells with the hole and the electron polaron, respectively, and $E[\mathrm{MAPb}_{1-\mathrm{x}}\mathrm{Sn}_{\mathrm{x}}\mathrm{I}_3]$ the total energy of the pristine system. Then, we define the polaron binding energies as $E_b(h^+) = \mu(h_{\mathrm{loc}})$ and $E_b(e^-) = \varepsilon_{\mathrm{C}} - \mu(e_{\mathrm{loc}})$ where ε_{C} is the conduction band edge of the pristine system.

Electrostatic finite size corrections for slabs are here taken into account with the Freysoldt-Neugebauer-Van de Walle (FNV) scheme.[19, 21] In particular, for charged surfaces, we employ the formulation proposed by Komsa and Pasquarello.[22] This scheme allows for a separation of the spurious interactions between the periodically repeated charges and the interactions between physical image charges occurring because of the variation in the dielectric constant across the surface. The energy correction is given as $E_{corr}^{q} = E_{iso} - E_{per} + q\Delta V$, where E_{per} is the electrostatic energy calculated for a model representing the employed supercell, E_{iso} the electrostatic energy obtained when uniformly scaling all the dimensions of the supercell, and ΔV the shift in the electrostatic potential between the model and the DFT calculation.

S3. Structural models of bulk and surfaces

We here consider the tetragonal phase of $\mathrm{MAPb}_{0.5}\mathrm{Sn}_{0.5}\mathrm{I}_3$ which is stable at room temperature. While metal halide perovskites usually undergo a transition from tetragonal to pseudo-cubic phase at high temperature, the observed A-site cation disorder and electronic properties were found to be very similar.[23, 24] Therefore, the electronic properties observed by our electronic-structure calculations performed on the tetragonal phase and its associated surfaces are fairly representative of the system under operative conditions.

For slab calculations, we focus on the (001) surface since both theoretical calculations[25, 26] and X-ray diffraction experiments[27] indicate that this is one of the dominant facets in tetragonal MAPbI_3. We note that the arrangement of MA in the slab models is such that the direction of the molecular dipoles is alternated (cf. the MA molecules along the *x* direction in Fig. 1 of the main text), thus implying that the net dipole field is minimal along the *z* direction.

For calculations of bulk models of $MAPb_{0.5}Sn_{0.5}I_3$, we employ a 2×2×2 supercell ($a = b = 17.71$ Å, $c = 25.07$ Å) corresponding to the experimental density. Slab models consist of 408 atoms, $a = b = 17.71$ Å, $c = 50$ Å, with c including a vacuum layer of ∼ 25 Å. Calculations of the surface of tetragonal $MAPbI_3$ are performed on a 5-layers 408-atoms slab terminated with lead diiodide (PbI_2). The simulation cell has $a = b = 17.70$ Å, $c = 50$ Å, including a vacuum layer of 25 Å. The adequacy of the slab models employed in this work has been extensively tested in previous publications against slab thickness. [6, 7, 28] We here further verify that our results are not affected by the surface area. We perform supplementary calculations on a larger model of surface 1. In particular, we evaluate if the considered model induces spurious interactions among periodic replicas of defective species. To this end, we employ a 1632-atoms slab, with $a = b = 35.42$ Å, $c = 50$ Å, with c including a vacuum layer of ∼ 25 Å. We then calculate the polaron binding energy for the hole polaron and evaluate the charge localization in comparison with those achieved with the smaller model extensively employed in this work. Our results show that the binding energy is essentially retained when calculated for the larger model of the surface (cf. Fig. S1), in agreement with previous observations for bulk $MAPbI_3$.[29] Then, we also consider IFD formation and we verify that the charge localization and the total-energy difference between the model bearing the IFD and that with two semi-localized extra holes [$\Delta E(I\mathrm{FD}) = E(\mathrm{IFD}) - E(2h^+)$] are essentially unmodified when calculated for the larger model (cf. Fig. S2 and Table S1). The calculated density of states for models of different sizes are also found to be consistent (cf. Fig. S3).

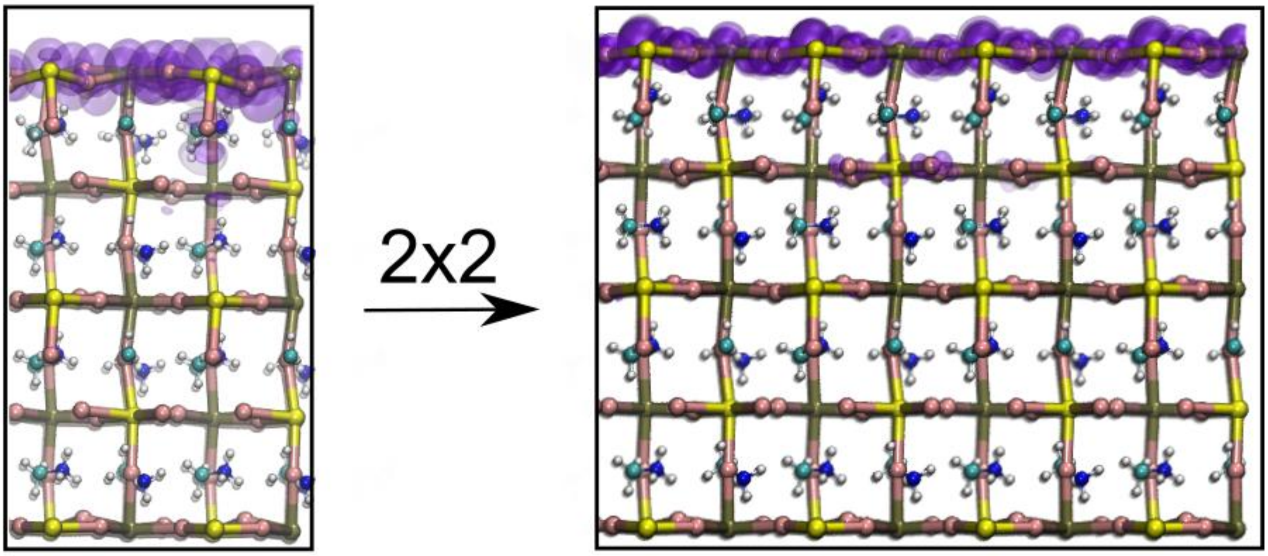

Figure S1. representation of a surface hole polaron on (left) the structural model of surface 1 employed in the main text and on (right) a 2x2 surface model. Pb atoms are given in brown, Sn in yellow, I in pink, C in cyan, N in blue, and H in white, isodensity representation of the hole in purple. The z axis lies vertically.

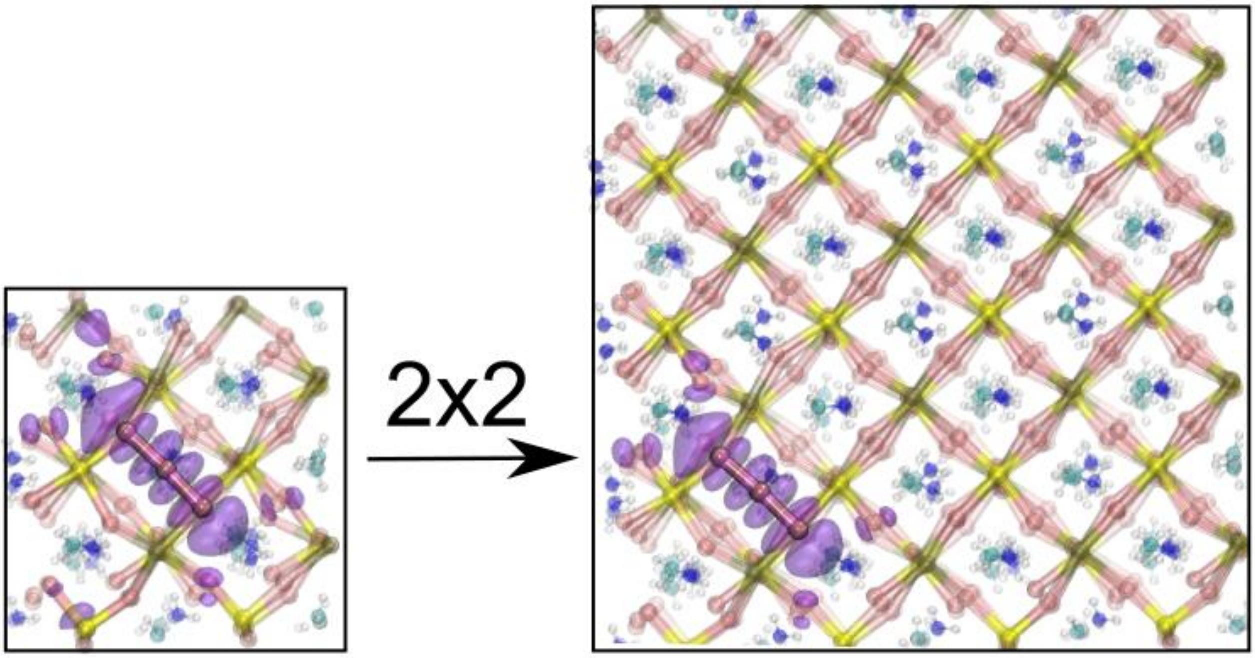

Figure S2. Top view representation of a iodine Frenkel defect on (left) the structural model of surface 1 employed in the main text and on (right) a 2x2 surface model. Pb atoms are given in brown, Sn in yellow, I in pink, C in cyan, N in blue, and H in white, isodensity representation of the hole in purple. The I atoms belonging to the tri-iodide moiety are highlighted.

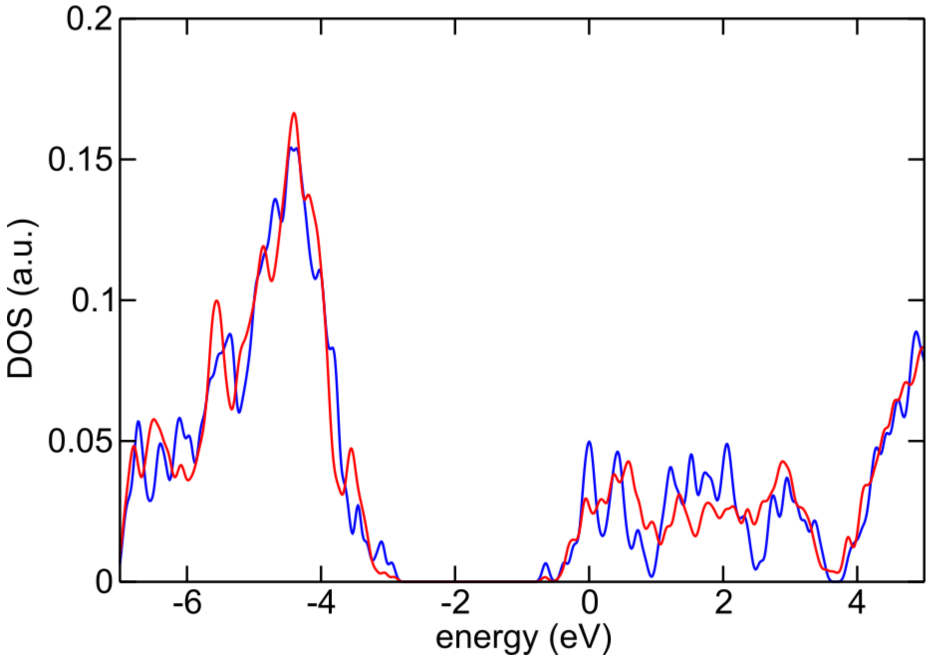

Figure S3. Electronic density of states (DOS) calculated at PBE0+rVV10 level of theory showing the valence band and the bottom of the conduction bands for models of surface 1 bearing an IFD. The DOS for the 408-atoms slab is represented in blue while that for the 1632-atom slab is given in red.

Table S1. Calculated values of $E_b(h^+)$ and $\Delta\mathrm{E}(\mathrm{IFD})$ for models of the (001) surface of $\mathrm{MAPb_{0.5}Sn_{0.5}I_3}$ of different size. For definitions, cf. text. All values are given in eV.

N of atoms	$\boldsymbol{E_b(h^+)}$	$\boldsymbol{\Delta\mathrm{E}(\mathrm{IFD})}$
408	0.22	−0.81
1632	0.21	−0.75

S4. Hole localization in bulk $MAPb_{0.5}Sn_{0.5}I_3$ and at selected surfaces

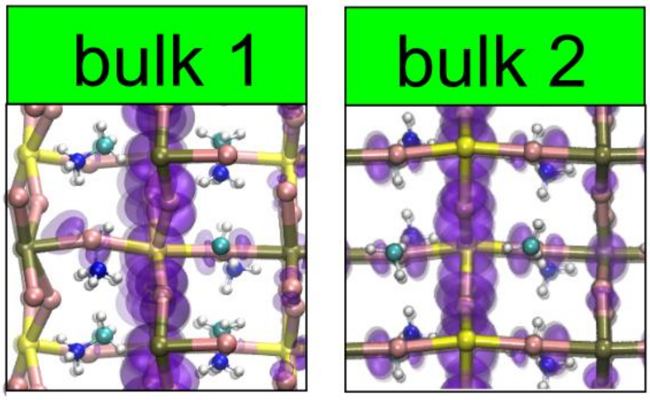

Figure S4. Isodensity representation of hole polaron on bulk 1 (left panel) and bulk 2 (right panel) models of tetragonal $MAPb_{0.5}Sn_{0.5}I_3$. The tetragonal axis lies horizontally. Pb atoms are given in brown, Sn in yellow, I in pink, C in cyan, N in blue, and H in white, isodensity representation of the hole in purple.

For both bulk and surface models, we consider:

(i) hole polaron formation and the respective binding energy.

(ii) V-center formation (cf. main text) for which we define $\Delta E(\mathrm{V}) = E(\mathrm{V}) - E(h^+)$ as the total-energy difference between the bulk/surface model bearing the V-center and that with a semi-locolized hole polaron.

(iii) IFD formation (cf. main text) for which we define $\Delta E(I\mathrm{FD}) = E(\mathrm{IFD}) - E(2h^+)$ as the total-energy difference between the bulk/surface model bearing the IFD and that with two semi-localized extra holes.

(iv) oxidation of Sn(II) to Sn(IV) for which we define $\Delta E(\mathrm{Sn}) = \mathrm{E}[\mathrm{Sn(IV)}] - E(2h^+)$ as as the total-energy difference between the bulk/surface model bearing a surface Sn(IV) and that with two semi-localized extra holes

For bulk 1 and bulk 2 models, we observe formation of a hole polaron (cf. Fig. S4) with charge localization on SnI_2 and $Pb_{0.5}Sn_{0.5}I_2$ surfaces with a binding energy of 0.12 and 0.14 eV (cf. Table S2), respectively, in line with a previous study, with the slight difference ascribed to the different methodology employed.[30] When studying the V-center, we observe that the Sn-bridging I_2^- is ~0.15 eV more stable than the Pb-bridging one. However, even the lowest energy V-center still feature $\Delta E(\mathrm{V})$ values of ~0.50 eV for both models of bulk $MAPb_{0.5}Sn_{0.5}I_3$ (cf. Table S2) Therefore, formation of a V-center upon trapping of a single hole is highly unfavourable, in line with previous calculations on $MAPbI_3$.[7] We then consider IFD formation. We find that an IFD on a SnI_2 plane is 0.27 eV more stable than on a PbI_2 plane for bulk 2 model. However, even the lowest-energy IFD features $\Delta E(\mathrm{IFD})$ =0.89 eV, its formation being substantially unfavoured. Finally, no oxidation of Sn(II) to Sn(IV) is envisaged for both the models of the bulk material as pristine systems do not possess the environment required to induce Sn(IV) species.[31]

Table S2. Calculated values of $E_b(h^+)$, $\Delta\mathrm{E(V)}$, $\Delta\mathrm{E(IFD)}$ and $\Delta\mathrm{E(Sn)}$. For definitions, cf. text. All values are given in eV.

Mixed perovskite	$\boldsymbol{E_b(h^+)}$	$\boldsymbol{\Delta E(\mathrm{V})}$	$\boldsymbol{\Delta \mathrm{E(IFD)}}$	$\boldsymbol{\Delta E(\mathrm{Sn})}$
Bulk 1	0.14	0.48	−0.89	//
Surface 1	0.22	0.17	−0.81	−0.89
Bulk 2	0.12	0.49	0.90	//
Surface 2	0.23	0.27	−0.58	−0.55
Surface 3	0.12	0.30	0.23	//

We then study surface 2 model (cf. main text). A single injected hole is found to be localized as surface hole polaron on a terminal SnI_2 plane (cf. Fig. S5), in line with results showed in the main text for surface 1. Analysis of the energetics of V-center, IFD and of surface Sn(IV) produce results in agreement with those discussed in the main text for surface 1, with values slightly shifted by the higher valence band edge of the SnI_2-terminated slab.

In contrast, for the surface 3 model, the polaron is localized on a sub-terminal SnI_2 plane with a binding energy of 0.12 eV [cf. Table S2 and Fig. S5], close to the bulk value. Both the V-centers and

IFD are found to be unstable with $\Delta E(\mathrm{V}) = 0.30$ eV and $\Delta \mathrm{E}(\mathrm{I}_3^-) = 0.23$ eV, respectively. In this regard, PbI_2 coverage appears to induce an effect very similar to that observed upon MAI coverage on the surface of lead halide perovskites, i.e. it hinders formation of charge-trapping species while, however, preventing hole transfer on the surface.[6]

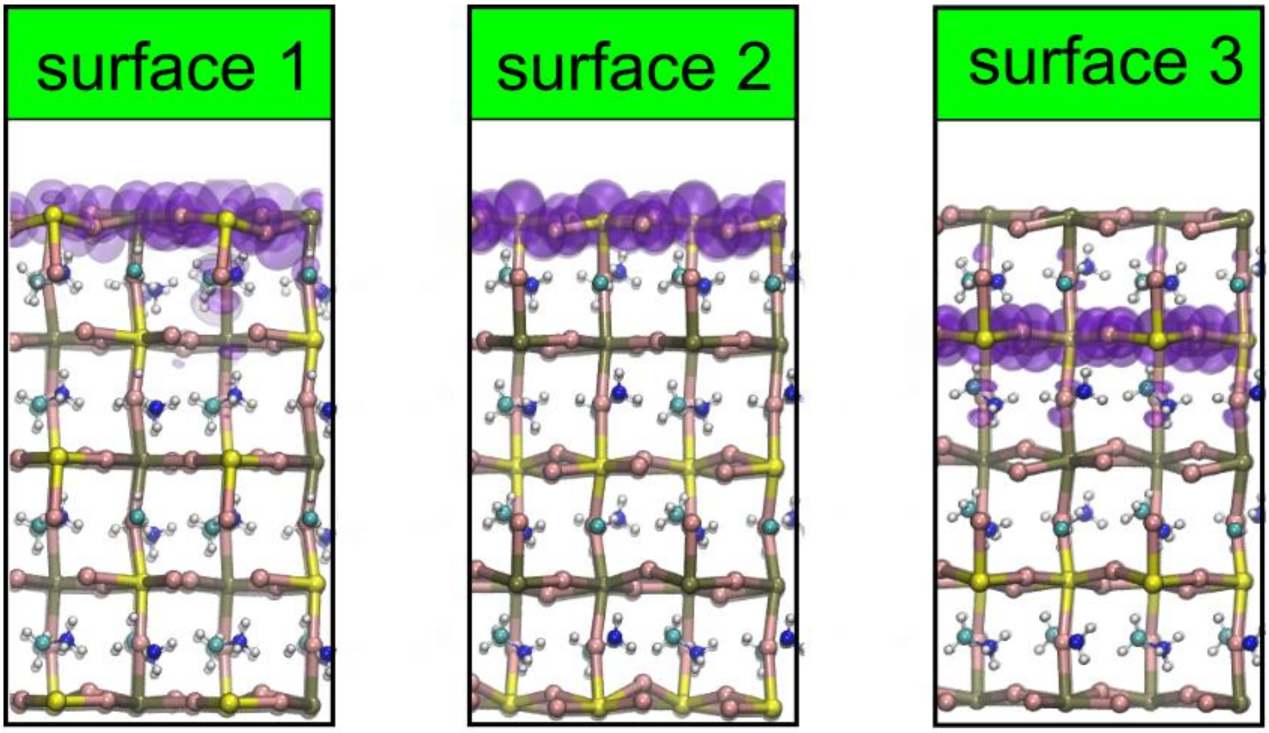

Figure S5. Isodensity representation of hole polaron on the surface 1 (left panel), surface 2 (middle panel), and surface 3 models of the (001) surface of $MAPb_{0.5}Sn_{0.5}I_3$. Pb atoms are given in brown, Sn in yellow, I in pink, C in cyan, N in blue, and H in white, isodensity representation of the hole in purple. The z axis lies vertically.

S5. Effect of Sn/Pb clustering on the energetics of slabs and hole localization.

In order to assess the stability of different Sn/Pb distributions, we construct three new slab models starting from the surface 1 model employed in the main text. In particular, we build models by (i) exchanging the position of a surface Sn and Pb atom (Clust1), (ii) increasing the content of Sn on the surface by exchanging a surface Pb with a sub-surface Sn (Clust2) and (iii) decreasing the content of

Sn on the by exchanging a surface Sn with a sub-surface Pb (Clust3). In all the cases, the modifications have been performed on both the sides of the slab. Clust1 is found to be 0.03 eV more stable than the parent surface 1 slab, thus suggesting that the two arrangements are essentially equivalent. We find that increasing (decreasing) surface Sn content is slightly favourable (unfavourable) as Clust2 (Clust3) is 0.11 (0.06) eV more (less) stable than the original slab. Overall, from these results, we infer that different rearrangements are close in energy and that Sn occurrence on the surface should be favoured.

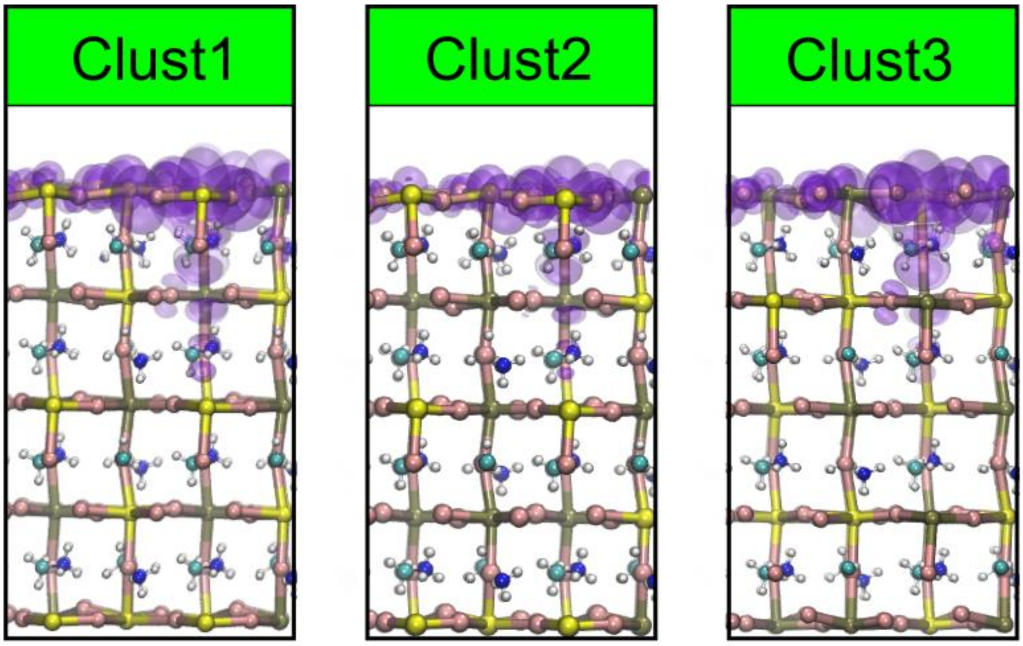

Figure S6. Isodensity representation of hole polaron for Clust1-3 models of the (001) surface of $MAPb_{0.5}Sn_{0.5}I_3$. Pb atoms are given in brown, Sn in yellow, I in pink, C in cyan, N in blue, and H in white, isodensity representation of the hole in purple. The z axis lies vertically.

We then investigate the hole polaron on the constructed models. For all considered models, hole localization occurs on the terminal metal-iodide plane, with energetics essentially equivalent to those calculated for surface 1 model (cf. Fig. S6 and Table S3).

Table S3. Calculated values of $E_b(h^+)$ for surface 1 and Clust1-3 models of the (001) surface of $MAPb_{0.5}Sn_{0.5}I_3$. For definitions, cf. text. All values are given in eV.

Model	$\boldsymbol{E_b(h^+)}$
Surface 1	0.22
Clust1	0.17
Clust2	0.20
Clust3	0.22

S6. Schematic representation of hole trapping on surface Sn vacancy and I interstitial

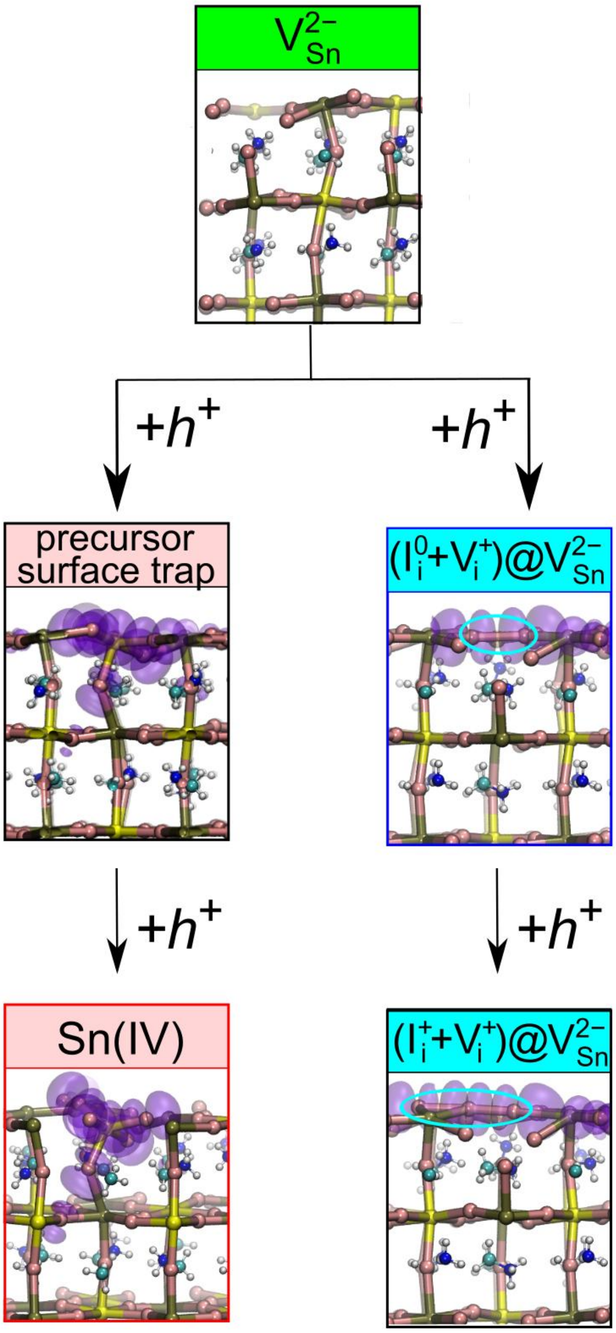

Figure S7. Schematic representation of hole-trapping species on the (001) $Pb_{0.5}Sn_{0.5}I_2$ surface of $MAPb_{0.5}Sn_{0.5}I_3$ bearing a Sn vacancy. Pb atoms are given in brown, Sn in yellow, I in pink, C in cyan, N in blue, and H in white, isodensity representation of the hole in purple. The z axis lies vertically.

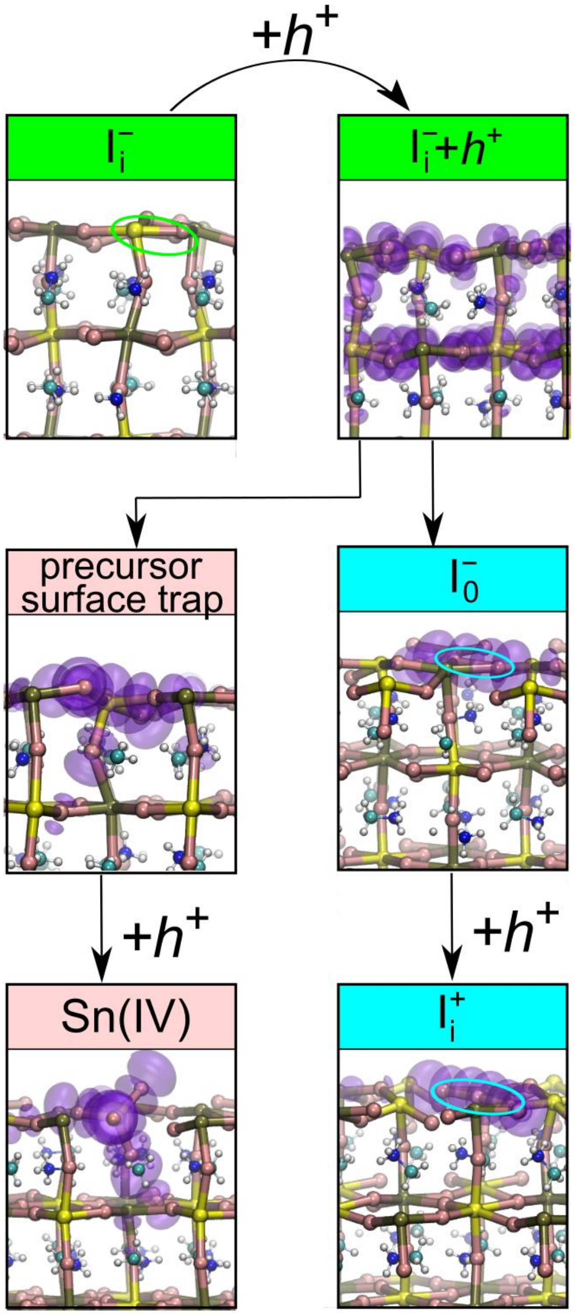

Figure S8. Schematic representation of hole-trapping species on the (001) $Pb_{0.5}Sn_{0.5}I_2$ surface of $MAPb_{0.5}Sn_{0.5}I_3$ bearing a I interstitial. Pb atoms are given in brown, Sn in yellow, I in pink, C in cyan, N in blue, and H in white, isodensity representation of the hole in purple. The z axis lies vertically.

S7. Electron localization in bulk $MAPb_{0.5}Sn_{0.5}I_3$ and at selected surfaces.

Table S4. Calculated values of $E_b(e^-)$ for bulk $MAPb_{0.5}Sn_{0.5}I_3$ and selected surfaces. All values are given in eV.

System	$\boldsymbol{E_b(e^-)}$
Bulk (layered)	0.04
PbI_2 surface	0.02
SnI_2 surface	0.02
Bulk (diagonal)	0.04
$Pb_{0.5}Sn_{0.5}I_2$ surface	0.04

We here discuss the physics of extra electrons in $MAPb_{0.5}Sn_{0.5}I_3$. We first verify that, upon injection of a single electron in the bulk material or at selected surfaces, no localization is envisaged. The added electron is found to be essentially delocalized in all the cases with negligible binding energies (cf. Table S4). Therefore, we consider possible electron-trapping defects such as the iodine vacancy $\mathrm{V_I}$ and interstitial tin $\mathrm{Sn_i}$.[32] We here again focus on surface 1 model. Electron-trapping in halide perovskites can be associated with the formation of metallic dimers. For $\mathrm{V_I}$, we observe the formation Pb-Sn bond (cf. Fig. S9) through the following reaction:

$$\mathrm{Pb^{2+}@V_I} + \mathrm{Sn^{2+}@V_I} + 2e^- \rightarrow \mathrm{PbSn^{2+}@V_I} \qquad \text{(S7)}$$

Similarly, electrons could be captured by an interstitial Sn with the creation of a dimer $\mathrm{Sn_2^+}$ (cf. Fig. S9):

$$\mathrm{Sn_i^{2+}} + \mathrm{Sn^{2+}} + 2e^- \rightarrow \mathrm{Sn_2^+} \qquad \text{(S8)}$$

However, when accounting for spin-orbit coupling in the calculations, the narrowing of the band gap, mainly induced by the shift in the conduction band edge, brings the charge transition levels associated with $\mathrm{V_I}$ and $\mathrm{Sn_i}$ outside the band gap of perovskite (cf. Fig. S7). Furthermore, we note the formation energy of surface V_I is higher than of its bulk counterpart, which implies that a lower concentration of surface V_I is expected. In contrast, surface Sn_i is sensitively stabilized with respect to the bulk, a result that can be explained with the larger reconstruction available on the surface to accommodate the extra tin atom.

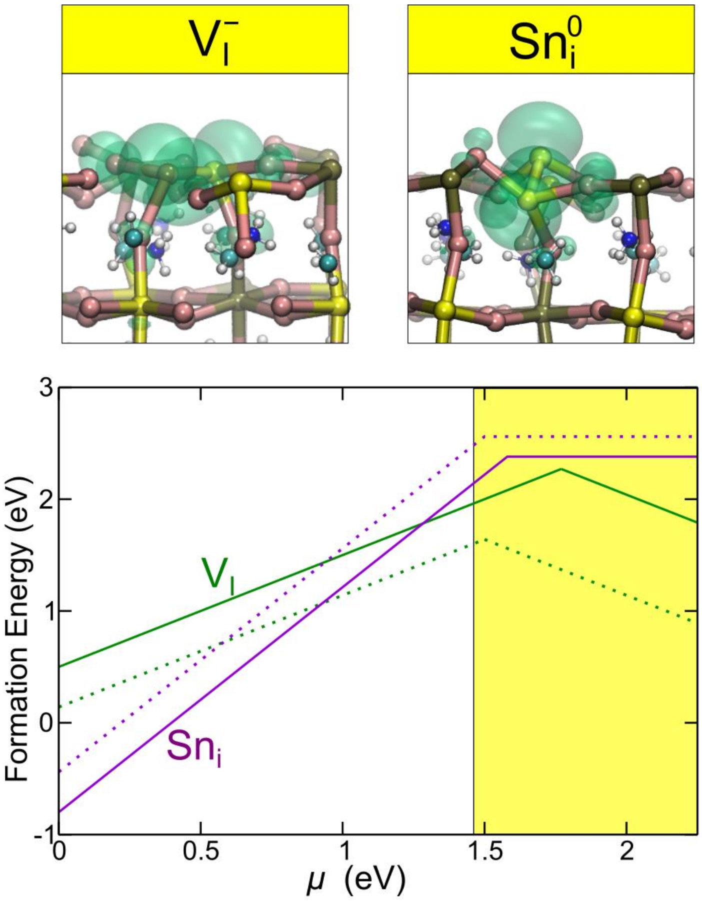

Figure S9. (upper panels) Isodensity representation (green) of the highest occupied molecular orbitals of V_I^- and Sn_i^0 on the (001) surface of $MAPb_{0.5}Sn_{0.5}I_3$ and (lower panel) formation energies of V_I and Sn_i as a function of the electron chemical potential μ. Dashed lines for the respective values calculated for the bulk material. The yellow shaded area highlights the region above the conduction band of the material calculated at the hybrid+SOC level of theory. We consider iodine medium conditions (cf. main text).

References

1. Perdew, J. P.; Ernzerhof, M.; Burke, K., Rationale for mixing exact exchange with density functional approximations. *The Journal of chemical physics* **1996,** *105* (22), 9982-9985.
2. Adamo, C.; Barone, V., Toward reliable density functional methods without adjustable parameters: The PBE0 model. *The Journal of chemical physics* **1999,** *110* (13), 6158-6170.
3. Vydrov, O. A.; Van Voorhis, T., Nonlocal van der Waals density functional: The simpler the better. *The Journal of chemical physics* **2010,** *133* (24), 244103.
4. Sabatini, R.; Gorni, T.; De Gironcoli, S., Nonlocal van der Waals density functional made simple and efficient. *Physical Review B* **2013,** *87* (4), 041108.
5. Perdew, J. P.; Parr, R. G.; Levy, M.; Balduz, J. L., Density-Functional Theory for Fractional Particle Number: Derivative Discontinuities of the Energy. *Physical Review Letters* **1982,** *49* (23), 1691-1694.
6. Ambrosio, F.; Meggiolaro, D.; Mosconi, E.; De Angelis, F., Charge localization and trapping at surfaces in lead-iodide perovskites: the role of polarons and defects. *Journal of Materials Chemistry A* **2020,** *8* (14), 6882-6892.
7. Ambrosio, F.; Mosconi, E.; Alasmari, A. A.; Alasmary, F. A. S.; Meggiolaro, D.; De Angelis, F., Formation of colour centres in lead-iodide perovskites: Self-trapping and defects in bulk and surfaces. *Chemistry of Materials* **2020**.
8. VandeVondele, J.; Krack, M.; Mohamed, F.; Parrinello, M.; Chassaing, T.; Hutter, J., Quickstep: Fast and accurate density functional calculations using a mixed Gaussian and plane waves approach. *Computer Physics Communications* **2005,** *167* (2), 103-128.
9. Goedecker, S.; Teter, M.; Hutter, J., Separable dual-space Gaussian pseudopotentials. *Physical Review B* **1996,** *54* (3), 1703.
10. VandeVondele, J.; Hutter, J., Gaussian basis sets for accurate calculations on molecular systems in gas and condensed phases. *The Journal of Chemical Physics* **2007,** *127* (11), 114105.
11. Guidon, M.; Hutter, J.; VandeVondele, J., Auxiliary Density Matrix Methods for Hartree−Fock Exchange Calculations. *Journal of Chemical Theory and Computation* **2010,** *6* (8), 2348-2364.
12. Even, J.; Pedesseau, L.; Jancu, J.-M.; Katan, C., Importance of Spin–Orbit Coupling in Hybrid Organic/Inorganic Perovskites for Photovoltaic Applications. *The Journal of Physical Chemistry Letters* **2013,** *4* (17), 2999-3005.
13. Umari, P.; Mosconi, E.; De Angelis, F., Relativistic GW calculations on CH3NH3PbI3 and CH3NH3SnI3 Perovskites for Solar Cell Applications. *Scientific Reports* **2014,** *4*, 4467.
14. Im, J.; Stoumpos, C. C.; Jin, H.; Freeman, A. J.; Kanatzidis, M. G., Antagonism between Spin–Orbit Coupling and Steric Effects Causes Anomalous Band Gap Evolution in the Perovskite Photovoltaic Materials CH3NH3Sn1–xPbxI3. *The Journal of Physical Chemistry Letters* **2015,** *6* (17), 3503-3509.
15. Giannozzi, P.; Baroni, S.; Bonini, N.; Calandra, M.; Car, R.; Cavazzoni, C.; Ceresoli, D.; Chiarotti, G. L.; Cococcioni, M.; Dabo, I.; Dal Corso, A.; de Gironcoli, S.; Fabris, S.; Fratesi, G.; Gebauer, R.; Gerstmann, U.; Gougoussis, C.; Kokalj, A.; Lazzeri, M.; Martin-Samos, L.; Marzari, N.; Mauri, F.; Mazzarello, R.; Paolini, S.; Pasquarello, A.; Paulatto, L.; Sbraccia, C.; Scandolo, S.; Sclauzero, G.; Seitsonen, A. P.; Smogunov, A.; Umari, P.; Wentzcovitch, R. M., QUANTUM ESPRESSO: a modular and open-source software project for quantum simulations of materials. *Journal of Physics: Condensed Matter* **2009,** *21* (39), 395502.
16. Hamann, D. R., Optimized norm-conserving Vanderbilt pseudopotentials. *Physical Review B* **2013,** *88* (8), 085117.
17. Halgren, T. A.; Lipscomb, W. N., The synchronous-transit method for determining reaction pathways and locating molecular transition states. *Chemical Physics Letters* **1977,** *49* (2), 225-232.

18. Ambrosio, F.; Meggiolaro, D.; Mosconi, E.; De Angelis, F., Charge Localization, Stabilization, and Hopping in Lead Halide Perovskites: Competition between Polaron Stabilization and Cation Disorder. *ACS Energy Letters* **2019,** *4* (8), 2013-2020.

19. Komsa, H.-P.; Rantala, T. T.; Pasquarello, A., Finite-size supercell correction schemes for charged defect calculations. *Physical Review B* **2012,** *86* (4), 045112.

20. Freysoldt, C.; Grabowski, B.; Hickel, T.; Neugebauer, J.; Kresse, G.; Janotti, A.; Van de Walle, C. G., First-principles calculations for point defects in solids. *Reviews of Modern Physics* **2014,** *86* (1), 253-305.

21. Freysoldt, C.; Neugebauer, J.; Van de Walle, C. G., Fully Ab Initio Finite-Size Corrections for Charged-Defect Supercell Calculations. *Physical Review Letters* **2009,** *102* (1), 016402.

22. Komsa, H.-P.; Pasquarello, A., Finite-Size Supercell Correction for Charged Defects at Surfaces and Interfaces. *Physical Review Letters* **2013,** *110* (9), 095505.

23. Poglitsch, A.; Weber, D., Dynamic disorder in methylammoniumtrihalogenoplumbates (II) observed by millimeter-wave spectroscopy. *The Journal of Chemical Physics* **1987,** *87* (11), 6373-6378.

24. Guan, L.; Xu, X.; Liang, Y.; Han, S.; Guo, J.; Wang, J.; Li, X., Effect of atomic configuration on band gap behaviour in CH3NH3SnxPb1−xI3 perovskites. *Physics Letters A* **2020,** *384* (8), 126173.

25. Haruyama, J.; Sodeyama, K.; Han, L.; Tateyama, Y., Termination Dependence of Tetragonal CH3NH3PbI3 Surfaces for Perovskite Solar Cells. *The Journal of Physical Chemistry Letters* **2014,** *5* (16), 2903-2909.

26. Haruyama, J.; Sodeyama, K.; Han, L.; Tateyama, Y., Surface Properties of CH3NH3PbI3 for Perovskite Solar Cells. *Accounts of Chemical Research* **2016,** *49* (3), 554-561.

27. Baikie, T.; Fang, Y.; Kadro, J. M.; Schreyer, M.; Wei, F.; Mhaisalkar, S. G.; Graetzel, M.; White, T. J., Synthesis and crystal chemistry of the hybrid perovskite (CH3NH3)PbI3 for solid-state sensitised solar cell applications. *Journal of Materials Chemistry A* **2013,** *1* (18), 5628-5641.

28. Meggiolaro, D.; Mosconi, E.; Proppe, A. H.; Quintero-Bermudez, R.; Kelley, S. O.; Sargent, E. H.; De Angelis, F., Energy Level Tuning at the MAPbI3 Perovskite/Contact Interface Using Chemical Treatment. *ACS Energy Letters* **2019,** *4* (9), 2181-2184.

29. Meggiolaro, D.; Ambrosio, F.; Mosconi, E.; Mahata, A.; Angelis, F. D., Polarons in Metal Halide Perovskites. *Advanced Energy Materials* **2020,** *10* (13), 1902748.

30. Mahata, A.; Meggiolaro, D.; De Angelis, F., From Large to Small Polarons in Lead, Tin, and Mixed Lead–Tin Halide Perovskites. *The Journal of Physical Chemistry Letters* **2019,** *10* (8), 1790-1798.

31. Ricciarelli, D.; Meggiolaro, D.; Ambrosio, F.; De Angelis, F., Instability of tin iodide perovskites: Bulk p-doping vs. surface tin oxidation. *ACS Energy Letters* **2020**.

32. Meggiolaro, D.; Ricciarelli, D.; Alasmari, A. A.; Alasmary, F. A. S.; De Angelis, F., Tin versus Lead Redox Chemistry Modulates Charge Trapping and Self-Doping in Tin/Lead Iodide Perovskites. *The Journal of Physical Chemistry Letters* **2020,** *11* (9), 3546-3556.